

**ELECTROSPUN FUCOIDAN LOADED PCL/PEO
NANOFIBER SCAFFOLDS FOR SMALL
DIAMETER VASCULAR GRAFTS**

A DISSERTATION

*Submitted in partial fulfillment of the
requirements for the award of the degree*

of

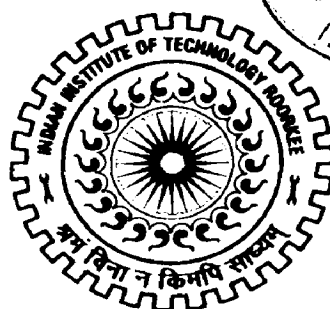
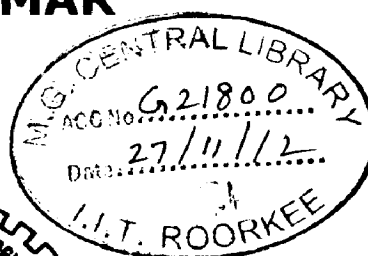
MASTER OF TECHNOLOGY

in

NANOTECHNOLOGY

By

S.UDAY KUMAR

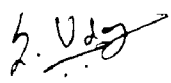


**CENTER OF NANOTECHNOLOGY
INDIAN INSTITUTE OF TECHNOLOGY ROORKEE
ROORKEE -247 667 (INDIA)
JUNE, 2012**

CANDIDATE'S DECLARATION

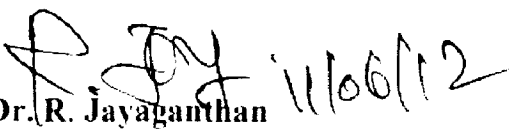
I hereby declare that the work which is being presented in dissertation entitled **"Fucoidan Loaded PCL-PEO Nanofiberous Scaffolds for Small Diameter Vascular Grafts"** submitted in partial fulfillment of the requirement for the award of degree of **Master of Technology in Nanotechnology**, submitted in the **Centre of Nanotechnology, Indian Institute of Technology Roorkee**, is an authentic record of my own work carried out under the guidance of **Dr. R. Jayaganthan**, Associate Professor, Department of Metallurgical and Materials Engineering and **Dr. N. C. Mishra**, Assistant Professor, Department of Paper Technology, Indian Institute of Technology Roorkee.

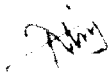
Date: 10.6.2012
Place: Saharanpur


S. Uday kumar
Enrollment No. – 10551015
M.Tech (2nd Year)
Centre of Nanotechnology
Indian Institute of Technology Roorkee

CERTIFICATE

This is to certify that the above declaration made by the candidate is correct to best of my knowledge and belief.


Dr. R. Jayaganthan
Associate Professor
Department of Metallurgical &
Materials Engineering
Indian Institute of Technology Roorkee


Dr. N. C. Mishra,
Assistant Professor
Department of Paper Technology
Indian Institute of Technology Roorkee

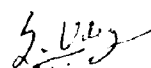
ACKNOWLEDGMENT

I am deeply indebted to my guide Dr. N.C. MISHRA, Assistant Professor, Department of Paper Technology, and Dr. JAYAGANTHAN, Associate Professor, Department of Material and Metallurgy for improvising a potential thrust within me, for pursuing a comprehensive project work on **“FUCOIDAN LOADED PCL-PEO NANOFIBEROUS SCAFFOLDS FOR SMALL-DIAMETER VASCULAR GRAFTS”**. Their impeccable contribution in guiding me at every hurdle that I faced meanwhile, has led me to the successful culmination of the aforementioned work to the best possible extent.

I am deeply indebted to Dr. Anil Kumar and Dr. S.K. Nath Head of the Department, who modeled us both technically and morally for achieving greater success in life. I express my deepest gratitude to the same, for giving me permission to reside and work at Saharanpur campus, Department of Paper and Pulp Technology, Indian Institute of Technology Roorkee for this semester.

I express my sincere thanks to Research Scholar Rajan Walia Sir, Institute Instrumentation Centre, for his kind support in SEM analysis of the samples.

At last but none the least, I take this opportunity to extend my deep appreciation to my friends, for their helpful and kind disclosure towards me throughout this course work.


S. UDAY KUMAR

Publications

Book chapter:

- (1) Uday Kumar, Sweta Gupta, Sneh Gautam, Chhavi Sharma, and Narayan Chandra Mishra "Production of nanofibers by electrospinning and their application in engineering and technology"- **National conference on Nanoscience and Nanobiotechnology-ISBN: 978-81-922112-1-3.**

Conference Proceedings:

- (1) Uday kumar, Narayana Chandra Mishra, and Jayaganthan R, "Fucoidan loaded PCL-PEO nanofiberous scaffolds for Small Diameter Vascular Grafts"- **International conference NANOBIO-2012 Cochin.**

Table of Contents

Candidates declaration	II
Acknowledgements	III
Publications	IV
Table of Contents	V
Abstract	VIII
Abbreviations	IX
List of Tables	X
List of Figures	XI

Chapter 1

Introduction

(1.1) Background.....	1
(1.2) Thesis objectives.....	6

Chapter 2

Literature Review

(2.1) Historic review of Small Diameter Vascular Grafts.....	8
(2.2) Challenges of artificial SDVG.....	10
(2.3) Rationale of constructing tissue engineered vascular grafts.....	10
(2.3.1) Natural vascular structure.....	10
(2.3.2) Mechanical properties.....	13
(2.3) Potential of polymer nanofibers as tissue engineered scaffolds.....	13
(2.3.1) Electrospinning.....	13
(2.3.2) Nanofiber scaffolds.....	15
(2.3.4) Cells-nanofiber scaffolds interaction.....	16

Chapter 3

Materials and Methods

(3.1) Extraction and Characterization of Fucoidan.....	19
(3.1.1) Extraction of Fucoidan from brown seaweed <i>Sargassum weitti</i>	19
(3.1.2) Confirmatory APTT assay for Fucoidan in the extract.....	20
(3.1.3) FTIR confirmation and characterization for extracted Fucoidan.....	20
(3.1.4) Estimation of amount of Fucoidan extracted.....	20
(3.2) Electrospinning setup.....	21
(3.2.1) Optimization of PEO/PCL nanofibers by electrospinning.....	22
(3.2.1.1) Taguchi Method - Design of Experiments.....	22
(3.2.1.2) ANOVA analysis.....	27
(3.3) Fabrication of SDVG with Fucoidan loaded luminal surface.....	28
(3.4) Fabrication of Fucoidan loaded bi-layered vascular graft like conduit.....	29
(3.4) Study of interface and dimensional uniformity.....	30
(3.5) FTIR characterization of Fucoidan loaded nanofibers.....	30
(3.6) Study of Fucoidan release profile from the bi-layered.....	30

Chapter 4

Results and Discussion

(4.1) Extraction and Characterization of Fucoidan.....	32
(4.1.1) Extraction of Fucoidan from brown seaweed <i>Sargassum weitti</i>	32
(4.1.2) FTIR confirmation and characterization for extracted Fucoidan	33
(4.1.3) Estimation of Fucoidan extracted from <i>Sargassum weitti</i>	34
(4.2) Fiber diameter and Morphology.....	36
(4.2.1) Range analysis by Taguchi DOE.....	42
(4.2.2) Analysis of variance for fiber diameter with respect to each parameter.....	44
(4.2.3) Regression analysis.....	46
(4.3) Characterization of Fucoidan loaded PEO/PCL nanofiber.....	46
(4.3.1) Fiber morphology.....	46
(4.3.2) FTIR characterization of Fucoidan loaded nanofiber.....	47

(4.4) Bilayered Fucoïdan loaded SDVG.....	49
(4.5) Cross-sectional uniformity of the bi-layered graft prepared.....	50
(4.6) Degradation of PEO/PCL nanofiber.....	52
(4.6.1) DSC analysis.....	52
(4.7) Fucoïdan release profile from bi-layered vascular graft.....	53
(4.8) Conclusion.....	60
Reference.....	61

Abstract

The prime stumbling block for achieving prolonged patency of SDVG (<6 mm in diameter) is to forgo the high incidence of arteriosclerosis, thrombosis and re-stenosis, specially its major pathology, arterial intimal hyperplasia. Intimal hyperplasia arises from migration and proliferation of vascular smooth muscle cells (VSMCs). Intimal hyperplasia accounts for around 40% (late implantation) failure of the SDVG (small diameter vascular graft). Though there have been well established results for the potential of Fucoidan as a drug for intimal hyperplasia there has not been any attempt to impregnate Fucoidan into the vascular stents which can thereby aid in successful long term patency of SDVG. Hence, in this work Fucoidan is sought after for its potential in improving SDVG patency by inculcating it in PEO/PCL nanofibrous scaffold of SDVG. Fucoidan, a sulfated polysaccharide is now a well established drug with anti-coagulant, anti-complimentary, anti-oxidant, anti-tumor, anti-viral properties, apart from this the therapeutic potential of Fucoidan being effectuated is reduction of neo-intimal hyperplasia.

At first, Fucoidan is extracted from the brown sea weed *Sargassum wightii* by slight modification of acid hydrolysis method. The extracted Fucoidan was confirmed by FTIR and APTT assay. After which, the PEO/PCL blend composition, and the operating parameters of electrospinning for producing uniform PEO/PCL nanofibrous scaffold were established by Taguchi (Orthogonal array) DOE. The parameters thus obtained were then adopted for fabricating First and Second layer of bi-layered graft like conduit, the intermediate layer (i.e. one between first and second) of the graft is a Fucoidan loaded PEO/PCL layer, formed by electrospaying Fucoidan loaded PEO/PCL polymer blend. Thus, the conduit fabricated is a bi-layered graft, in which a Fucoidan loaded PEO/PCL layer sandwiched between two layers of PEO/PCL nanofibers. The Fucoidan release profile from the bi-layered vascular conduit was monitored in vitro. The Fucoidan release profile depicted a sustained and uniform release profile after a small initial burst; hence it

was established that this system can serve the purpose of delivering drugs in latter phase of SDVG implantation.

To establish the significance of drug loading in the intermediate layer drug release profile from Fucoidan loaded monolayered conduit is also monitored. The comparison of which indicated that the release profile of the graft fabricated can be tuned according to the requirement by varying the depth of drug loaded layer across the conduit cross-sectional thickness. Once the Fucoidan loaded nanofiberous scaffold attains the mechanical compliance and cell compatibility it would of critical importance in SDVG fabrication.

Abbreviations

3-D: three-dimensional

ANF: aligned nanofiber meshes

ATR-FTIR: attenuated total reflectance Fourier transform infrared

BM: basement membrane

BNF: collagen-blended P(LLA-CL) nanofiber meshes

BSA: bovine serum albumin

CAMs: cell adhesion molecules

CMFDA: 5-chloromethyl fluorescein diacetate

DCM: Dichloromethane

DMF: *N,N*-dimethylformamide

ECs: endothelial cells

ECM: extracellular matrix

EPCs: endothelial progenitor cells

E-selectin: endothelial leucocyte adhesion molecules-1

FBS: fetal bovine serum

FITC: fluorescein isothiocyanate

GAGs: glycosaminoglycans

HCAECs: human coronary artery endothelial cells

HCASMCs: human coronary artery smooth muscle cells

PCL: polycaprolactone

PEO: Polyethyleneoxide

List of Tables

Table 1.1: Drug eluting vascular grafts in market

Table 1.2: Other drug that are inculcated in vascular stents

Table 3.1: Composition of L-Fucose standard solutions

Table 3.2: Different factors and levels of each factors taken into consideration

Table 3.3: Composition of different PEO/PCL and Chloroform:Acetic acid solution

Table 3.4: Generating vectors tabulation (L9) for Taguchi DOE

Table 3.5: Taguchi DOE for PEO/PCL fiber diameter optimization

Table 4.1: Response of clotting time with change in Fucoidan concentration

Table 4.2: Absorbance with change in concentration of L-Fucose

Table 4.3 : Fiber diameter and morphology for L9 Taguchi DOE

Table 4.4: Analysis of 20 fiber diameter observation from 2000X image of the sample

Table 4.5: Dimentional uniformity across the length and the cross-section at different points along the length

Table 4.6: Amount of Fucoidan released from bi-layered conduit with course of incubation time in PBS

Table 4.7: Percentage drug release from bi-layered conduit with diameter of 5.515mm and thickness of 0.165mm

List of Figures

Fig1.1: Schematic outline for the study: step 1, fabrication of nanofiber meshes (NFM); step 2, evaluation of the *in vitro* Endothelialization on the flat NFM; step 3, constructing the blood vessel-like 3-D tubular nanofiber scaffold with the lumen seeded with ECs.

Fig 2.2: Electrospinning set up [42].

Fig 3.1: Procedure for Taguchi Analysis by Minitab 16.

Fig 4.1: Plot of Clotting time with amount of Fucoidan (micrograms), almost a linear raise in clotting time is observed with increase in quantity of Fucoidan. Implying that the major component of the fraction extracted is Fucoidan.

Fig 4.2: FTIR analysis of the fraction extracted and its correspondence to the groups present in Fucoidan

Fig 4.3: Plot of absorbance with increase in concentration of Fucoidan, this standard graph was used to interpret the Fucoidan concentration in the fraction extracted.

Fig 4.4: SEM images of PEO-PCL polymer nanofibers with composition as 20% acetic acid and 80% chloroform solvent system and 1:2 PEO/PCL 20ml (g/20ml) of PEO-PCL.(a) Orientation of the fibers (b) surface morphology of the fiber.

Fig 4.5: SEM images showing the fiber morphology variation with respect to PEO/PCL composition.(a) 1:2 PEO/PCL in 20ml of (10% acetic acid and 90% chloroform), (b) 1:1 PEO/PCL in 20ml of (10% acetic acid and 90% chloroform).

Fig 4.6: PEO-PCL nanofibers prepared by electrospinning 1:2 wt% in 20ml solvent of 20% acetic acid and 80% chloroform(a) at lower magnification,(b) at higher magnification.

Fig 4.7: Fiber diameter calculation by Materials Plus 12.

Fig 4.8: Main effects for (A)Means and (B) SN ratio.

Fig 4.9: Fucoidan loaded PEO/PCL intermediate layer.

Fig 4.10: FTIR of (1) Pure Fucoidan (2) PEO-PCL nanofibers and (3)Fucoidan loaded PEO-PCL nanofibers.

Fig 4.11: Cross sectional view of (a) single layered PEO/PCL nanofiberous graft, (b) bi-layered PEO/PCL conduit with the intermediate being loaded with Fucoidan and sandwiched between the first and second layer.

Fig 4.12: DSC of (1)initial PEO/PCL nanofibers ,(2) 4hrs PBS incubated PEO/PCL nanofibers, (3) 12 days PBS incubated PEO/PCL nanofiberous samples.

Fig 4.13: Plot of (a) Means with standard error and (b) Box plot with percentage Fucoidan release with time.

Chapter 1

Introduction

(1.1) Background:

Coronary heart disease peripheral vascular disease, Atherosclerosis and heart disease all together account for 51% of cardiovascular death and morbidity [1]. The major therapy for coronary heart disease is to bypass the blocked artery using autologous blood vessels, such as internal mammary artery or saphenous vein. Synthetic blood vessels prostheses are successfully being used for large-diameter vascular reconstruction. However, until now, no functional small-diameter (< 6 mm) artificial blood vessel is available, due to thrombus formation early after implantation. Although endothelial cell seeding in small-diameter vascular prosthesis improves the patency to some extent, this approach has not resulted in large-scale clinical applications. Therefore, tissue engineering of small-diameter vascular constructs is an expanding area of research.

The ideal tissue-engineered vascular construct should be prepared from a biocompatible material that degrades and re-sorbs at a controlled rate, to match cell and tissue ingrowth *in vitro* and/or *in vivo*. The material should be processable into a porous tubular scaffold with interconnected pores, which allows cell adhesion, thus providing a suitable environment for cell growth and transfer of nutrients, gases and metabolic end products. The mechanical properties of the resulting construct should match those of a native artery, especially in terms of compliance, to avoid the development of intima hyperplasia after implantation and subsequent vascular failure

In the past, many attempts to produce a successful tissue-engineered small-diameter vascular construct have been made using either collagen gels [2-5] or synthetic materials [5]. Only 15-30% of small-diameter synthetic vascular grafts remain open (or patent) after 5 years [6]. The rate of thrombosis (static aggregation of blood factors) occurred in synthetic vascular grafts is greater than 40% in the early phase after 6 months followed by continuous intimal hyperplasia (excessive tissue ingrowth and plasma protein depositions) in the chronic phase[7]. Thrombosis and intimal hyperplasia are caused by host tissue foreign body responses, initiated first by plasma protein depositions, followed by leukocytes and platelets adhesion and migration of endothelial cells (ECs) and smooth muscle cells (SMCs) onto the lumen of vascular grafts. Effects of these factors will even be amplified in a low flow rate and high resistance small-diameter vascular graft, resulting in easier graft occlusion and subsequent failure. It is to this challenge that vascular tissue engineering is seeking to answer. One of the commonly accepted methods for developing tissue engineered small-diameter vascular grafts is to hybridize vascular grafts made from biodegradable materials with vascular cells[8,9,10].

Small diameter vascular grafts made out of synthetic biomaterials have been unsuccessful as they have been associated with high incidence of thrombosis (11). The failure of SDVG in traversing its course from a table top product to bed side product is attributed to either one or a combination of the following complications, high incidence of infection, aneurysm, anastomosis at the site of graft clamping, secondary atherosclerosis, fibrosis, mechanical incomppliance etc(12,13,14). Most of these pathological complications which lead to failure of graft are instigated by a cascade of events starting from cellular scale, and one such discernable aberration in characteristics of cell is manifested as neo-intimal hyperplasia(15,16).

Intimal hyperplasia is an unregulated regenerative response leading to migration and proliferation of vascular smooth muscle cells (VSMCs) when its endothelial layer (tunica intima) is tempered by any means(16). Intimal hyperplasia is set off by a rapid surge in release of certain signaling molecules by the endothelial cells (in tunica intima) which mediate over proliferation of SMC's in tunica media followed by, their migration towards tunica intima(17). The activation of nuclear factor (NF)- κ B has been found to be involved in

the process of neointimal hyperplasia, inciting growth factor-dependent activation of smooth muscle cell (SMC) proliferation, protease-dependent migration of cells to the wounded area, and cytokine-dependent matrix deposition. The SMC's once on their arrival at the luminal side of the vessel, secrete collagen, whose deposition facilitates the recruitment of fibrin molecules from circulating blood to the vicinity; this cascade of events eventually primes thrombosis and stenosis(18). Hence, potential to overcome intimal hyperplasia plays a vital role in determining long term patency of implanted SDVG.

On enumeration of pathological significance of neo-intima formation in success of SDVG, few physical techniques and drugs to regulate over proliferation of SMC's have been employed with diverse success rate, few of those which deserve mention are, use of high energy laser beam to burn or scrap off the accumulated SMC's over the luminal surface(19), use of angioplasty(20), and use of certain anti-proliferative drugs like paclitaxel(21), taxane(22), actinomycin D, and everolimus. A potent drug called Fucoidan which is very much analogous (functionally) to those mentioned previously is now a well established therapeutic compound for its potential in resolving intimal hyperplasia. It is a sulfated polysaccharide with diverse therapeutic potential range, as anti-coagulant anti-complimentary, anti-oxidant, antitumor, anti viral properties and anti-proliferative. The therapeutic index for each its potential varies according to the source and composition of Fucoidan. The source of Fucoidan adapted in this work is a brown sea weed "Sargassum weitti" procured from the shores of Gulf of Munnar. Fucoidan had a stronger antithrombotic activity than heparin. Further, vascular cells treated with fucoidan demonstrated a decrease in proinflammatory cytokine and chemokine production as well as inhibition of proliferation (intimal hyperplasia).

Each kind of drug has its own biological half-life and cannot maintain an effective concentration for a long time. Merely increasing the dose of drug will extend itself into the toxic response region, whereas taking the selected dose of drug for several times during a period of time (e.g. three times a day) is not convenient for the patient. To overcome such barriers and improve the amount of drug delivered at the target site there has been attempts to inculcate these therapeutic drugs to the stent itself as sited in the table.

Table 1.1: Drug eluting vascular grafts in market.

Product	Components of the stent	Company	Drug inculcated
CYPHER	316L stainless steel (low-magnetic, low-carbon) and are coated with a mixture of two polymers(PEVA AND PBMA), parylene C.	Cordis, Johnson and Johnson.	Sirolimus
TAXUS	316L stainless steel and is coated with the Translute polymer [poly (styrene-b-isobutylene-b-styrene)].	Boston Scientific.	Paclitaxel

Table 1.2: Other drugs that are inculcated in vascular stents.

Category of drug.	Drug	Company name	Clinical Trials
Rapamycin Derivatives	SIROLIMUS	Cordis	RAVEL/SIRUS
	<i>Tacrolimus</i>	JOMED	-----
	<i>Everolimus</i>	Guidant	FUTURE I/II/III
	<i>ABT-578</i>	Medtronic Abbott	ENDEAVOR
Taxol Derivatives	<i>Paclitaxel</i>	Boston Scientific	TAXUS I/II/III/IV
	<i>Batimistat</i>	Bio Compatibles	BRILLIANT
	<i>Actinomycin D</i>	Guidant	ACTION
Others	<i>Batimistat</i>	Bio Compatibles	BRILLIANT
	<i>Dexamethosone</i>	BiodivYsio	STRIDE
	<i>Actinomycin D</i>	Guidant	ACTION

In spite of such appreciable results in the use of Fucoïdan in overcoming intimal hyperplasia there have been no attempts to inculcate the drug in the vascular stent, so this work is pursued with an aim to fabricate a Fucoïdan loaded nanofiberous SDVG. In tandem with the drug mediated improvement of SDVG patency, fabrication of certain physical features (i.e. surface patterning) can provide a positive edge over conventional SDVG's. It include fabrication of graft surface with nano-scale features which can well mimic the ECM of the SMC's, and thereby aid in better integration of seeded cells to the biomaterial. The better the merge at the biomaterial and cell interface better is the scope of the grafts for long term patency.

A successful vascular graft can also be fabricated with nano-patterened surfaces so as to provide suitable scaffold for better proliferation and migration of SMC's, this in recent past has been well accomplished by fabrication of nano-scale engineered surfaces whose dimensions mimic those of the ECM. One easier and versatile rout to attain such nanoscale constructs is by electrospinning. Electrospinning is a technique to produce nanofibers of polymers (synthetic and biopolymers) form their melts or solution. The great ease in controlling the dimensions of the fibers and short fabrication time has given it an edge over other conventional nano-fiber generation techniques. The morphology of the fiber depends on the operating parameters and the inherent properties of the polymer being used. On consideration of the kind of mechanical strength that is required for a vascular graft to sustain the blood pressure, PCL is attributed to serve that purpose. The lone drawback of PCL to serve as a component of the vascular graft is its hydrophobicity and to over come this blend of hydrophilic LMW PEO is supplemented to PCL. Apart from improving the hydrophilicity of the fibers PEO presence also improves the degradability rate so as to comply with normal tissue regenerative response.

With this as the basis a hybrid structure Fucoïdan loaded nanofiberous scaffold of the synthetic biopolymer polycrapolactone (PCL) and polyethylene oxide (PEO) was prepared. This drug loaded layer is sandwiched between two layers of nanofiberous PEO and PCL to form a bi-layered conduit like structure. Fucoïdan had a stronger antithrombotic activity than heparin. Further, vascular cells treated with fucoïdan demonstrated a decrease in proinflammatory cytokine and chemokine production as well as inhibition of proliferation.

Each kind of drug has its own biological half-life and cannot maintain an effective concentration for a long time. Merely increasing the dose of drug will extend itself into the toxic response region, whereas taking the selected dose of drug for several times during a period of time (e.g. three times a day) are not convenient for the patient.

In this case, drug controlled release formulations and devices exhibit particular advantage because they can maintain the desired drug concentration in blood for a long period of time without reaching a toxic level or dropping below the minimum effective level. The PEO-PCL system of polymers are the subject of analysis as each can render a specific favorable properties to the SDVG constructed out of it. PEO being hydrophilic provides better patency of the SDVG along with certain other favorable properties like control in blood flow, implication in controlling over proliferation of cells. With this as the basis the work is sought over to fabricate SDVG with a better patency and that being achieved by overcoming neo-intimal hyperplasia. The Fucoidan loaded graft is also verified for its mechanical compliance to the native vascular system through certain standard testing procedures.

1.1 Thesis objectives:

The purpose of this study is to construct biomimetic electrospun nanofiber scaffolds which mimic the extracellular matrix (ECM)/basement membrane (BM) (step 1), with the objective of achieving effective endothelialization of the Fucoidan loaded PEO-PCL nanofiber scaffolds in terms of viability, attachment, as well as to observe phenotypic and functional manifestation in response to Fucoidan(step 2), and the final goal of constructing blood vessel-like 3-D tubular nanofiber scaffolds with the anti-intimal hyperplasia lumen composed of Fucoidan loaded PEO-PCL for small-diameter vascular grafts (step 3). The outline for this study is shown in Fig 1.1.

Moreover we proposed to pursue the following specific aims in this study:

1. Extraction of Fucoidan form brown sea weed *S.wightii* and its characterization.
2. To design a solvent system for PEO-PCL polymer blend and thus arrive at attainment of PEO-PCL nanofiber.

Hypothesis:

PEO-PCL nanofiber scaffold can render desired hydrophilicity in addition to this PEO has favorable implication in suppressing intimal hyperplasia.

3. To fabricate PEO-PCL nanofiber meshes (NFM) with high levels of reproducibility in fiber diameter uniformity and orientation.
4. To produce fucoidan loaded nano-fibrous vascular conduit and study the drug distribution and release profile from thus prepared conduit.
5. To evaluate the patency of Ar75 smooth muscle cells over the fucoidan loaded PCL-PEO conduit.

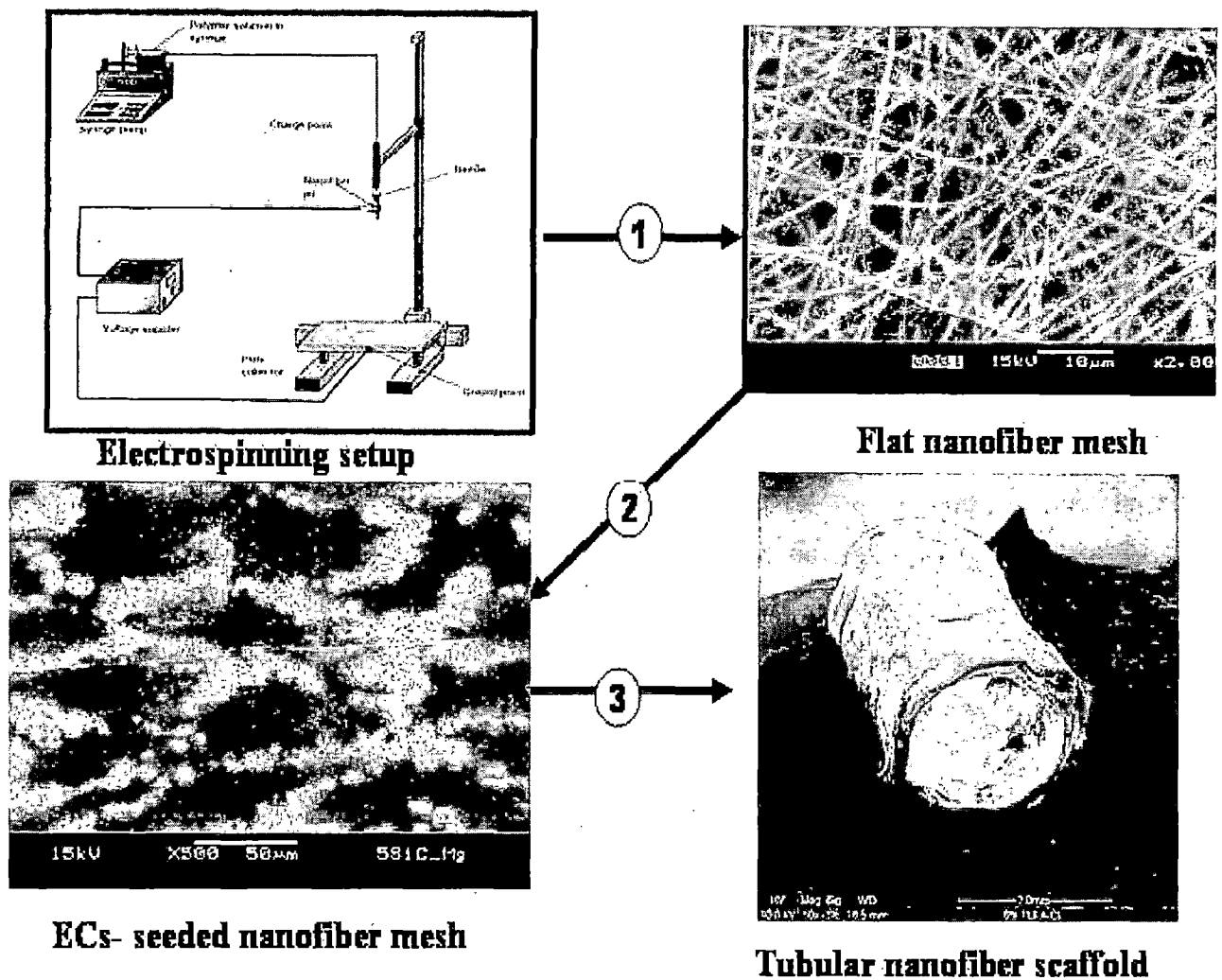


Fig 1.1. Schematic outline for the study: step 1, fabrication of nanofiber meshes (NFM); step 2, evaluation of the *in vitro* endothelialization on the flat NFM; step 3, constructing the blood vessel-like 3-D tubular nanofiber scaffolds with the lumen seeded with ECs.

Chapter 2

Literature Review

(2.1) Historic Review of Small Diameter Vascular Grafts

In 1993, L'Heureux et al. [23] prepared a TEBV using human cultured vascular cells and collagen and encountered the same mechanical challenge. In order to produce a TEBV with high burst strength, L'Heureux et al. [24] then took advantage of the abundant production of extracellular matrix (ECM) by mesenchymal cells (SMCs and fibroblasts) when cultured in the presence of vitamin C. In this work, an acellular ECM was synthesized human skin fibroblasts and upon dehydrated formed into a tubular sheet. This ECM sheet was wrapped around a polytetrafluoroethylene mandrel followed by a sheet of smooth muscle cells to form the basis of a vascular tube as the media. After maturation in a bioreactor for one week, a sheet of fibroblasts was wrapped around the construct to provide an adventitia. Following another maturation period of about 56 days, the inner mandrel was removed and endothelial cells were seeded onto the luminal side to construct a three-layered vascular graft characteristic of natural artery. To date, this approach is the most promising in small diameter vascular graft tissue engineering [25].

L'Heureux et al. then expanded this method by exclusively using autologous human cells. Their latest progress is using adult human fibroblasts extracted from skin biopsies to construct tissue-engineered blood vessels (TEBVs) that serve as arterial bypass grafts in long-term animal models. The patency and mechanic stability of this TEBV was proved through 8 months *in vivo* on animal models [26]; the grafts were mechanically sufficient for 21 months in human arterio-venous (A-V) shunt safety trails [27]. In addition, ~60% of these TEBVs maintained their primary patency for 6 months as A-V shunts for haemodialysis access, the

proportion of which is consistent with the value across all patient populations [28]. Very recently, they included other indications, such as the elastin enrichment by altering proteoglycan versican expression of SMCs to promote the synthesis and assembly of elastic fibers [29]. Currently, L'Heureux and colleagues are trying to shift their efforts toward shortening the generation time for this TEBV [27].

Other attempts by using natural materials to produce small diameter vascular grafts with improved mechanical properties are also impressive. For example, Nerem and coworkers [30, 31] extensively studied the interaction of collagen gel and vascular cells under both dynamic and static conditions. Constructs that underwent dynamic conditioning exhibited higher mechanical strength and increased tissue organization. More recently, they found that shear stress could induce the differentiation of embryonic stem cell toward endothelial like phenotype [32], which shed some light on addressing the ample needs of mature ECs in cardiovascular tissue engineering. Another interesting approach was the use of decellularized porcine small intestine submucosa (SIS) [33].

In this approach, SIS was coated with bovine fibrillar collagen and complexed with heparin at the luminal surface to reduce the potential for thrombosis. The underlying porcine collagen layer was crosslinked to mechanically support the construct. Strikingly, vascular cells (SMCs and ECs) became incorporated into these constructs during implantation. However, whether those vascular grafts with animal collagen are applicable to the human cardiovascular system remains uncertain and no further investigation has been reported. More recently, a study showed that decellularized porous collagen or elastin scaffolds could promote cell adhesion, proliferation and infiltration, yet the mechanical properties of these scaffolds need to be enhanced for this application [32]. The authors proposed to use bioreactor system to mechanically condition their cell-populated scaffolds and stimulate ECM synthesis, which waits for investigation. In conclusion, though decellularized scaffolds and cellular sheets are promising for inducing proper vascular cell activities, such as cell adhesion, proliferation and infiltration, they are often mechanically too weak to withstand pulsatile flow [32-34]. In most cases, natural materials or decellularized scaffolds were seeded with vascular cells to enhance the mechanical properties of the cell populated vascular grafts [31-33]. The time and cost

associated with the preparation of such grafts eliminates their potential for application in acute cases.

(2.2) Challenges of artificial SDVG:

The first synthetic vascular grafts used clinically were made of the woven fabric Vinyon N by Voorhees in 1952 [35]. From then on, a variety of materials including nylon, Orlon, PET (poly(ethylene terephthalate), Dacron®), ePTFE (expanded polytetrafluoroethylene, Teflon®), polyethylene, and polyurethane have been made into vascular grafts. For replacement of the abdominal aorta and iliac arteries, which have an inner diameter more than 6 mm, knitted Dacron® is the common choice, whilst for the femoropopliteal and femorotibial bypass, which have an inner diameter less than 6 mm, ePTFE is used together with knitted Dacron [36]. Although very inert, those materials do evoke host-tissue foreign body responses, initiated first by plasma protein deposition known as the Vroman effect [37], followed by leukocytes and platelets adhesion and the migration of endothelial and smooth muscle cell. These lead to thrombosis (static aggregation of blood factors) in the early phase followed by a continuous and intimal hyperplasia (excessive SMC ingrowth and plasma protein deposits) in the chronic phase. Thrombosis phenomenon will be more severe in small-diameter vascular grafts (inner diameter < 6 mm). This is because in small-diameter vascular grafts, blood pressure, resistance of blood flow, shear stress, and surface-to-volume ratio are high, which result in increased contact time of blood components with grafts and increased activation of blood coagulation (thrombosis)[38] As a result, small diameter synthetic vascular grafts suffer thrombosis rates greater than 40% after 6 months [39] and only 15-30% of them remain patent after 5 years[40]. The higher propensity of small-diameter vascular grafts to thrombosis has spurred the scientists to improve the standard materials and develop new materials. It is also to this challenge that tissue engineering approach is seeking to answer.

(2.3) Rationale of constructing tissue engineered vascular grafts

(2.3.1) Natural vascular structure

Current research on tissue engineered small-diameter vascular grafts focused more on the development of native blood vessel-like tubes (or conduits). The development of biomimetic

vascular grafts relies on the understanding of the anatomical structure and the biological functions of blood vessels. Normal blood vessels (except capillaries) have tri-lamellar structures, with each layer having specific functional properties (Fig 2.1). The intima (tunica intima) contains the endothelium, which is a single layer of ECs functioning to prevent spontaneous blood coagulation. As an interface between dynamic blood flow and static blood vessel wall, ECs are directly exposed to flow and the associated shear stress and blood pressure, which make ECs elongate in response to flow and orient their major axis with the direction of flow. Moreover ECs attach to a sub-endothelial layer which is a connective tissue bed, called the basement membrane (BM). This is adjacent to the internal elastic lamina which is a band of elastic fibers, found most prominently in larger arteries. The media layer (tunica media) is composed of smooth muscle cells (SMCs) and variable amount of connective tissues such as collagen, elastin, and proteoglycans. Specially, SMCs and collagen fibers have a marked circumferential orientation to withstand the higher pressures in the blood circulation, as well as their abilities to contract or relax in response to external stimulus. The adventitia layer (tunica adventitia) is composed primarily of fibroblasts and loose connective tissue fibers. In arteries with diameter greater than 1 mm, the innermost layer of the wall (intima) is nourished from blood flow in the lumen while the outer layers (the adventitia and part of the media) are supplied from small blood vessels called vasa vasorum.

The ECM in the vascular tissues forms a network composed primarily of collagen (mainly type I and III), elastin fibers, proteoglycans (including versican, decorin, biglycan, lumican, and perlecan), hyaluronan, and glycoproteins (mainly laminin, fibronectin, thrombospondin and tenascin). The mechanical properties critical to blood vessels' functions include tensile stiffness, compliance, elasticity and viscoelasticity. Collagen provides the tensile stiffness; elastin offer elastic properties; proteoglycans contribute to compressibility; the combination of all are responsible for the viscoelasticity property.

One important ECM structure in human body is the basement membrane (also called basal lamina), which is a flexible thin (40-120 nm thick) mat that underlie all epithelial cells (Fig 2.3) or endothelial cell sheets to separate them from the underlying connective tissue. In blood vessels, the basement membrane under the EC layer is mainly composed of EC-

secreted type IV collagen and laminin nanofibers embedded in heparin sulfate proteoglycan hydrogels. The basement membrane shows a nano- to submicron-scale topography of ECM macromolecules, including fiber mesh, pores, ridges, grooves, and peak valleys, which are also the features of the nanofiber scaffold. Therefore it makes sense to use the non-woven polymer nanofiber scaffold to construct the inner surface of vascular graft capable of quick endothelialization.

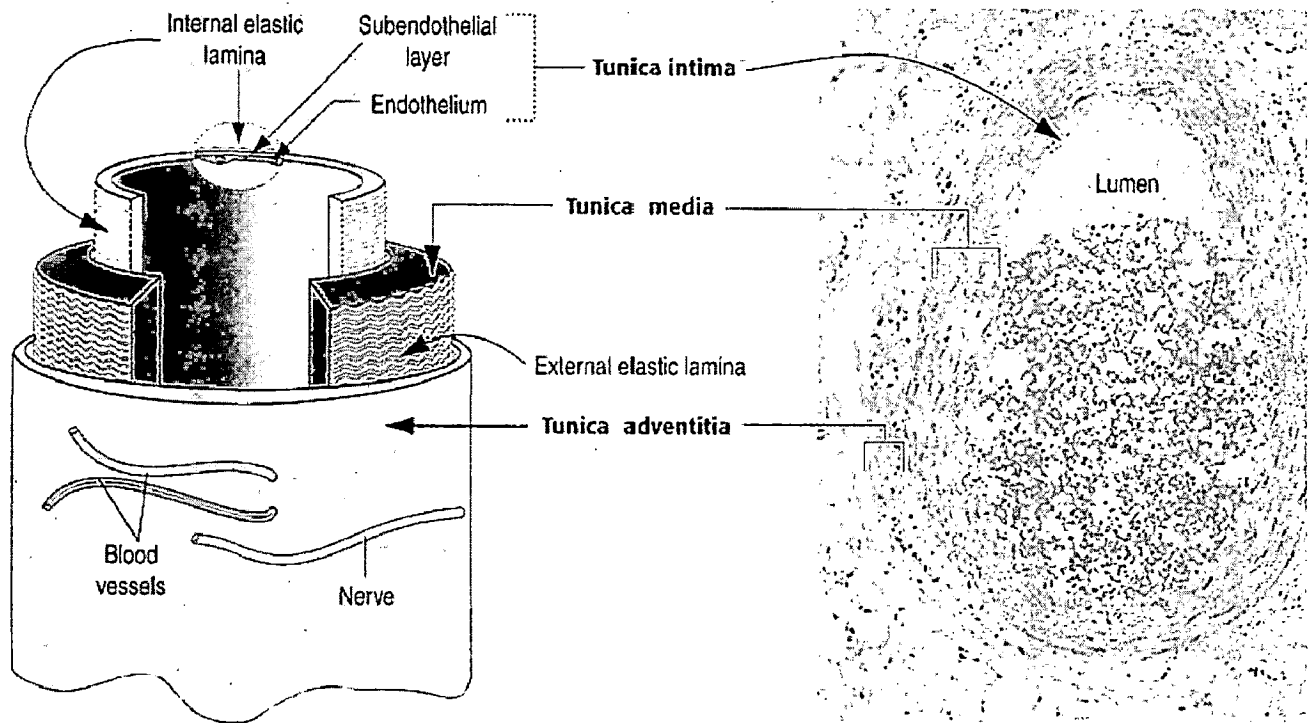


Fig 2.1: Schematic graph of the basic tri-lamellar structure of blood vessels.

Mimicking the three layer structure of native blood vessels has been the principle in tissue engineering approaches to design vascular grafts. Basically, three models have been used to construct the native-like tissue engineered vascular grafts using vascular cell types: 1) a mono-layer of EC seeded collagen gel; 2) a bi-layer of EC-monolayered intimal and SMC-inoculated medial layer; 3) a three-layer of EC, SMC, and fibroblasts. Results showed that three-layered vascular grafts had the highest potential of vascular wall regeneration, followed by the bi-layer vascular grafts. Robert Langer gave another criterion for the ideal tissue engineered vascular grafts: confluent endothelium, differentiated SMCs, sufficient mechanical integrity, and elastic modulus. It was found that the short-term patency of vascular grafts is highly dependent on the luminal surface properties while long-term patency

depends on mechanical properties of the grafts.

(2.3.2) Mechanical properties

Mechanical property is an important parameter to decide the long-term patency of vascular grafts. One of the main failure modes of vascular grafts is intimal hyperplasia especially at the anastomosis regions, which is believed to be associated with shear stress disturbances due to the compliance mismatch of the compliant artery and the rigid graft at the end-to-end anastomosis a). Most of the commercialized vascular grafts made from PET (Dacron™) and PTFE (Teflon™) are much less compliant (or too stiff) compared with that of the native blood vessels. This is one of the reasons for their lack of patency when used as the small-diameter vascular grafts. Besides compliance, vascular grafts should have sufficient tensile stiffness to withstand forces from the initial wound contraction and later tissue remodeling, as well as the physiological blood pressure (120 mmHg for typical systolic pressure). Although significant progress has been made, fabrication of vascular grafts with identical mechanical properties to those of native blood vessels remains an elusive goal. It should be highlighted, however, that a major advantage of tissue engineered vascular grafts is that they don't need to have mechanical properties identical to those of native blood vessels at implantation. Being composed of viable tissues with the potential to remodel, repair, and grow, tissue engineered vascular grafts should be theoretically able to completely adapt to local dynamic conditions and acquire the structure and mechanical features of the blood vessels, for which they replace.

(2.4) Potential of polymer nanofibers as tissue engineered scaffolds

(2.4.1) Electrospinning

Methods to produce nanoscaled polymeric fibers include electrospinning, self assembly, and phase separation, among which electrospinning is the most simple and efficient one. Electrospinning has been known for over seventy years. The patent of electrospinning was granted in 1902 in the USA [41]. Special needs in biomedical and other applications have stimulated renewed interests and studies on electrospinning since 1990s. Since then over 200

universities and research institutes worldwide have investigated various aspects of electrospinning. The number of patents applied for process and applications based on electrospinning are also growing over the years. Startups such as eSpin Technologies, NanoTechnics, and KATO Tech are just some companies that sought to reap the unique advantages offered by electrospinning while companies such as Donaldson have been using electrospun fibers in their air filtration products for the last two decades[42].

A key advantage of electrospinning to prepare ultra-fine polymer fibers is that almost any polymer with sufficiently high molecular weight that forms solution can be electrospun. Nanofibers made of natural polymers, polymer blends, nanoparticles or drug impregnated polymers and ceramic precursors have been successfully electrospun. Different fiber morphologies such as beaded fibers, ribbon fibers, porous fibers and core-shell, have also been spun[42]. The principle of electrospinning is to use an electric field to draw polymer solution or melt from an orifice to a collector. High voltages (10-20 kV) are used to generate sufficient surface charge to overcome the surface tension of the solution and a jet then erupts from the tip of the spinneret. The jet is only stable near the tip of the spinneret, after which the jet undergoes bending instability[43]. As the charged jet accelerates toward regions of lower potential, the entanglements of the polymer chain will prevent the jet from breaking up while the solvent evaporates resulting in fiber formation. Generally, a grounded plate is used to collect the fibers (Fig 2.3)[42].

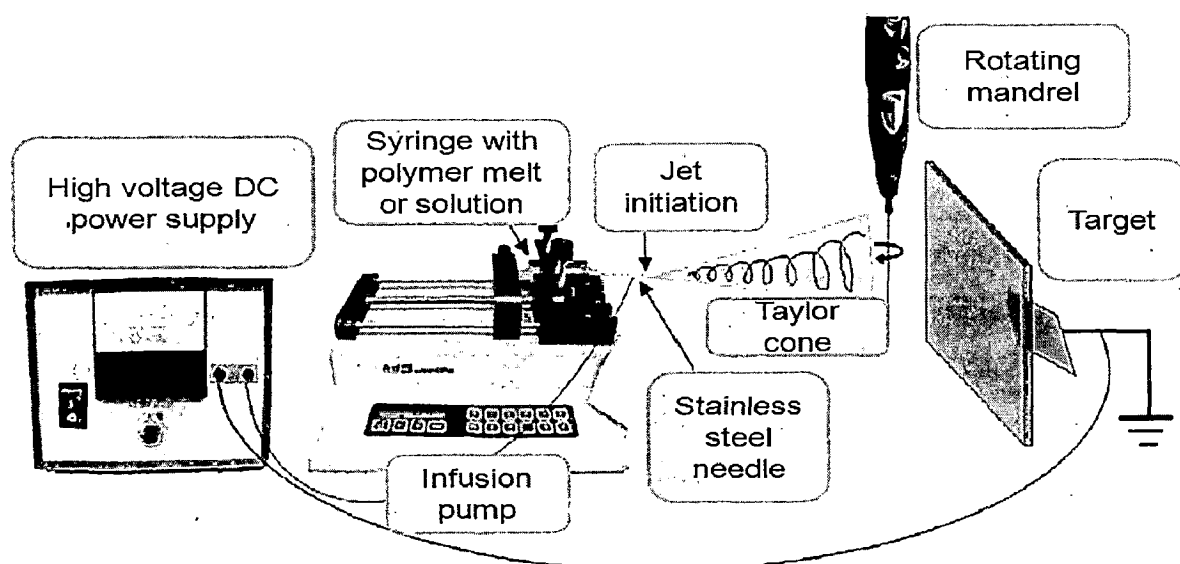
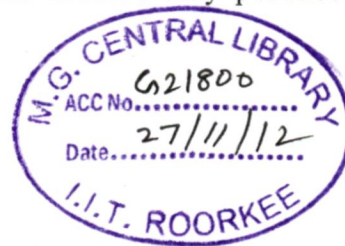


Fig 2.3: Electrospinning set up [42].

The diameters of the electrospun fibers are at least one order of magnitude smaller than those made by conventional extrusion techniques. Electrospinning usually produces non-woven sheet with a flat profile due to the ejection rate of the polymer solution through the orifice must be controlled at a low value if nanoscaled fiber diameter is desired. However, 3-D non-woven fibrous mesh can be obtained if the electrospinning time is long enough. Our experiences show that the thickness of the nanofiber increases with the electrospinning time at a typical speed of 20 $\mu\text{m}/\text{h}$. One effective method to increase the thickness of the nonwoven sheet is to use more than one orifice simultaneously, in which the electrospinning speed will be proportional to the number of the orifices. This method may produce 3-D nanofibrous scaffold in a short time in the future[44].

(2.4.2) Nano-fiber scaffolds



The principle of designing tissue engineered scaffolds is clear: the scaffold should mimic the structure and biological function of native extracellular matrix (ECM) as much as possible, both in terms of chemical compositions and physical structures. In terms of chemical compositions, ECM is mainly composed of three major classes of biomolecules: structural proteins like collagen and elastin, specialized proteins like fibronectin and laminin, and proteoglycans composed of a protein core and glycosaminoglycans (GAGs). In terms of physical structures, ECM is consisted of various protein fibrils interwoven within a hydrated network of GAG chains [45]. The function of the ECM is far more than providing a physical support for cells. It also provides a substrate with specific ligands for cell adhesion and migration, and regulates cellular proliferation and functions by storing and presenting various growth factors[46]. It is reasonably expected that an ECM-mimic tissue engineered scaffold may play a similar role to promote tissue regeneration *in vitro* as the native ECM does *in vivo*.

Polymer nanofiber scaffold is among the most promising biomaterials for native ECM analogues [44]. The potential of applying electrospinning in tissue engineered scaffolds is enormous since nanofiber scaffolds can mimic the nanoscaled dimension of the natural ECM and mesoscopic scale of ECM's spatial organization by controlling fiber's orientation and

spatial placement. Moreover, nanofiber scaffolds can emulate chemical compositions of ECM by including biomolecules into fibers. We found that there is a vivid similarity between the electrospun polycaprolactone (PCL) nanofiber scaffold and native ECM in rat cornea[47]. Another example is the apparent similarity between the electrospun collagen nanofibers and the ECM of the small intestine, which is composed of collagen bundles, in terms of both physical structure and chemical composition. In fact, non-woven microscaled polymer scaffolds have already been widely used in tissue engineering for a long time due to their high surface area and high porosity [48].

Electrospinning of the natural occurred biomaterials is much more challenging compared with the synthetic polymers for the difficulties in looking for appropriate solvent. 1,1,1,3,3,3-hexafluoro-2-propanol (HFP) is a commonly used solvent for electrospinning of proteins [49]. Electrospinning of silk fibroin has been performed with formic acid as the solvent[50]. The silk fibroin can also be mixed with PEO in water and electrospun, followed by washing with methanol to remove the PEO[51]. Huang *et al* prepared polypeptides containing repeated elastomeric peptide sequence of elastin by genetic engineering method. The polypeptide was dissolved in water and electrospun into nanofibers with diameter from 200 to 300 nm under appropriate conditions[52]. Fang X *et al* reported the electrospinning of calf thymus Na-DNA aqueous solutions with concentrations from 0.3% to 1.5% into nanofibers with diameters around 50 to 80 nm [53].

The simplicity and reproducibility of fabricating well-controlled polymer nanofiber scaffolds by electrospinning have invigorated big interests in the field of tissue engineering. In addition to the ECM-like architecture, polymer nanofibers have other desired features for tissue engineered scaffolds such as biocompatibility, high porosity for tissue ingrowth, high surface area-to-volume ratio, adjustable mechanical and biodegradable properties, capability of surface modification [53],and flexibility of loading drugs or genes [54].

(2.4.3) Cells-nanofiber scaffolds interactions

The reason why we need to study the interactions between cells and biomaterials *in vitro* is

based on the theory that “macroscopic tissue-level events are ultimately derived from, and thus could be controlled by, cellular and molecular level events at the tissue-implant interface” [55]. Thus any implant should be studied *in vitro* first before implantation *in vivo* for the interactions of cells and biomaterials in terms of cell adhesion, proliferation, phenotype maintenance, and functional development.

It has been well established that gross change in ECM affects cell behaviors. However little is known about how cell behaviors will be affected by fine changes at the nanometer scale in the synthetic ECM. Researchers as early as 1960s claimed that nanoscaled features influenced cell behaviors [56]. Cells attached and organized well around fibers with diameters smaller than size of cells[57]. Nanoscaled surface roughness with dimensions ranging from 20 to 50 nm produced by chemical etching on Silicone wafer enhanced neural cell adhesion and hydroxylase activity[58]. Nanoscaled surface topography has been found to promote osteoblast adhesions. Recent studies reported that osteoblast adhesion, proliferation, alkaline phosphatase activity, and ECM secretion on carbon nanofibers increased with decreasing fiber diameters in the range of 60-200 nm, while the adhesion of other cells like chondrocytes, fibroblasts, and smooth muscle cells was not affected. It has been postulated that the nanoscaled surface affects the conformation of the adsorbed adhesion proteins like vitronectin to affect the cell behaviors [59]. In addition, the nanoscaled dimension of the cell membrane receptors like integrins should also be considered.

Most of the works about *in vitro* cell culturing on nanofiber scaffolds was to evaluate cell adhesion, proliferation, gene expression and ECM secretion. Li *et al* cultured fibroblasts, cartilage and bone marrow derived mesenchymal stem cells on PLGA or PCL nanofibers[60]. It was found that the nanofiber scaffolds were capable of supporting cell attachment and proliferation. Fetal bovine chondrocytes were cultured on PCL nanofibers and their phenotype was evaluated. In addition to promoting phenotypic differentiation, the PCL nanofibers also promoted chondrocyte proliferation when the cultures were maintained in serum-containing medium. Adult bone marrow derived mesenchymal stem cells cultured in the PCL nanofibers were able to be induced to form chondrocytes in the presence of transforming growth factor (TGF- β 1), as evidenced by chondrocyte-specific gene

expressions and synthesis of cartilage-associated ECM proteins. The chondrogenic ability of the stem cells cultured in the PCL nanofibers was comparable to that observed for the stem cells maintained as cell aggregates or pellets.

Chapter 3

Materials and methods

(3.1) Extraction and Characterization of Fucoidan:

(3.1.1) Extraction of Fucoidan from brown seaweed *Sargassum weitti*:

The drug of interest – Fucoidan, was extracted from brown seaweed *Sargassum weitti* by slight modification of method adapted by Kim *et al.*. In brief, the weed was dried in hot air oven at 40°C for 48 hrs; and then ground down to fine chips roughly of around 2'*2' . This was subjected to acid hydrolysis by suspending them in 2 L of 0.1 N HCl for 24 h. Further the acid suspended chips were then sonicated in periodic intervals with following sonication parameters: Sonication power: 30W, Sonication duration: 3 mins, Sonication cycle interval: 5 mins, Number of sonication cycles: 5 cycles.

The resultant aqueous phase of the extract was separated from the rest by filtering the mixture through a fine meshed cloth followed by its neutralized with 1 N NaOH (pH – 7.2). Followed by this, the mixture is supplemented with 3 volumes of ethanol to precipitate the Fucoidan in the fraction. The mixture was allowed to stand for 24hrs to allow the precipitated mass to settle down (Fucoidan). The lower fraction of the extract is centrifugation for 10 min at 6000xg, the pellets obtained were re-suspended in water. The pH of the suspension was brought down to 2.0 with 1 N HCl and to this CaCl₂ added to the final concentration of 4 M CaCl₂ solution. The pellet was removed by centrifugation and the supernatant was treated with 3 volumes of ethanol. The ethanol precipitation was repeated twice and the pellets was re-dissolved in water, dialyzed (MWCO 14,000) at 4°C in water for 48 h and then freeze-dried. The final fraction was then confirmed to be Fucoidan by FTIR, APTT assay.

(3.1.2) Confirmatory APTT assay for Fucoidan in the extract:

Activated partial thromboplastin time (APTT) assays were carried out by the method of Andreson et al. Hundred μL of normal human platelet-poor plasma was mixed with 50 μL of a solution of purified fucoidan (0.1, 0.25, 1.0, 5.0 μg) and incubated for 2 min at 37°C. For control, equal volume of dH₂O was added instead of fucoidan solution. To the reaction mixture, 100 μL of APTT reagent was added and incubated for 2 min at 37°C and then 100 μL of 0.35 M CaCl₂ was added and the clotting time was noted.

(3.1.3) FTIR confirmation and characterization for extracted Fucoidan:

Fucoidan isolated from *Sargassum wightii* was characterized by FTIR to confirm its presence in the crude fraction obtained from the extraction process. The extracted fraction maintained at 45°C for 1 day to remove the moisture content present in it. The dried powder was then transferred to a vial and then carried forward for FTIR analysis. To the 2 mg of sample 1 gram of KBr was mixed in a mortar-pestle to obtain a homogenous mixture. Then the resultant mixture was struck between the presses to form a sheet like structure. After this it was transferred to the sample holder in the FTIR scanner, transmittance was measured from 400 cm^{-1} to 5000 cm^{-1} .

(3.1.4) Estimation of amount of Fucoidan extracted:

Fucose forms the major monosaccharide component of Fucoidan hence its estimation is taken as approximate estimation of Fucoidan. A standard graph of Fucose was prepared by phenol sulfuric acid method followed by measuring absorbance at 490 nm. With this as the standard the amount of Fucoidan in the fraction extracted was estimated. A 2mg of L-Fucose was purchased from Sigma Aldrich it was dissolved in 10ml distilled water to give a standard solution of concentration 200 micro-gram/ml. From this standard solution a gradient in concentration was developed by suitable dilution in separate tubes:

Add 6ml of concentrated sulfuric acid to each, immediately after these add 2 ml of 5% phenol to each of these solutions. The resultant solution is kept for incubation in water bath at 90°C for 5 min's. The solutions were taken out from the water bath, allowed to cool down to room temperature then its absorbance was measured at 330 nm. The compositions of each are

as follows:

About 50 gram's dry biomass of *Sargassum wightii* was taken for fucoidan extraction process. The final fraction obtained from the extraction process, which is crude fucoidan, weighed around 4 grams. A small portion 1 gram of this extract was carried forward with phenol-sulfuric acid method for estimation of L-Fucose content. The absorbance value thus obtained was then correlated to the standard graph of L-Fucose to obtain an approximate estimation of the Fucoidan content in the extracted fraction.

Table 2.1: Composition of L-Fucose standard solutions

S.N o.	Fucose (µg)	Volume of Standard (µL)	Water (µL)	Sulfuric acid (ml)	Phenol (ml)
1	200	1000	2000	6	2
2	300	1500	1500	6	2
3	400	2000	1000	6	2
4	500	2500	500	6	2
5	600	3000	0	6	2

(3.2) Electrospinning setup:

The electrospinning apparatus was equipped with a high-voltage power supply with maximal voltage of 50 kV. The PEO and PCL were dissolved in a mixture of acetic acid and chloroform as per DOE. The resultant blend is added in a 5-mL syringe attached to a 0.5mm diameter metal spinneret attached to its tip. A horizontal cylindrical counter electrode was located about 15 cm from the capillary tip; one of the ends of cylindrical collector was coupled to the axel of a motor regulated by a feedback system to control its revolution per minute. The flow rate of the polymer solution was controlled by a precision pump to maintain a steady flow from the capillary outlet. The experiment of temperature was controlled at 27°C, and the environment humidity was controlled between 45% and 50%. All the nonwoven fiber mats were vacuum dried at room temperature for 3 days to completely remove any solvent residue prior to further characterization.

(3.2.1) Optimization of PEO:PCL nanofibers by electrospinning:

Electrospinning is a very simple and versatile method of creating polymer-based high-functional and high-performance nanofibers. But most of the investigations are not systematic and describe the electrospinning process without quantitative accuracy. Inconsistent and even opposite results have been reported, which has hindered the consistent interpretation of the experiments. Orthogonal experimental (Taguchi method) method was used to investigate qualitative and quantitative correlations between fiber characteristics (diameters and morphologies) and the processing and materials parameter. Uniform fibers can be obtained without any beads by proper selection of the processing parameters, and a lower glass transition temperature was observed for electrospun fibers than that of native polymer.

(3.2.1.1) Taguchi Method - Design of Experiments

The solution properties and processing parameters for producing uniform PEO:PCL nanofibers by electrospinning were established through Taguchi DOE analysis (also called orthogonal array method of optimization). The factors taken into consideration for the optimization process were polymer proportion, solvent proportion, flow rate, and voltage. Three levels for each variable were taken up for the analysis on the basis of preliminary pilot experiments. Thus a four variable-three level (Table 5) orthogonal (L9) design of experiment (DOE) was adapted for the analysis.

The general steps involved in the Taguchi Method are as follows:

1. Define the process objective, or more specifically, a target value for a performance measure of the process. This may be a flow rate, temperature, etc. The target of a process may also be a minimum or maximum; for example, the goal may be to maximize the output flow rate. The deviation in the performance characteristic from the target value is used to define the loss function for the process.

2. Determine the design parameters affecting the process. Parameters are variables within the process that affect the performance measure such as temperatures, pressures, etc. that can be easily controlled. The number of levels that the parameters should be varied at must be specified. For example, a temperature might be varied to a low and high value of 40 C and 80

C. Increasing the number of levels to vary a parameter at increases the number of experiments to be conducted.

3. Create orthogonal arrays for the parameter design indicating the number of and conditions for each experiment. The selection of orthogonal arrays is based on the number of parameters and the levels of variation for each parameter, and will be expounded below.

4. Conduct the experiments indicated in the completed array to collect data on the effect on the performance measure.

5. Complete data analysis to determine the effect of the different parameters on the performance measure. With the above stated information and a reference to a paper dealing with optimization process using the same DOE, the range of parameters were set as required.

No of levels: 3 levels.

No of factors: 4 factors.

Table 2.2: Different factors and levels of each factors taken into consideration.

Levels	Factors			
	Polymer composition (PEO:PCL)	Solvent (Acetic acid: Chloroform)	Voltage (kV)	Flow rate (ml/hr)
Level 1	1:1	5:95	14	0.20
Level 2	1:2	10:90	16	0.25
Level 3	1:3	20:80	18	0.30

Table 2.3: Composition of different PEO:PCL and Chloroform:Acetic acid solution.

Levels	Polymer composition	Solvent	PEO	PCL	Chloroform	Acetic acid
			3.75% (g/ml)			
Level 1	1:1	5:95	0.375	0.375	1	19
Level 2	1:2	10:90	0.25	0.5	2	18
Level 3	1:3	20:80	0.1875	0.5625	4	16

The vector table L9 array is given as:

Table 2.4: Generating vectors tabulation (L9) for Taguchi DOE.

Experiment	Parameter 1	Parameter 2	Parameter 3	Parameter 4
1	1	1	1	1
2	1	2	2	2
3	1	3	3	3
4	2	1	2	3
5	2	2	3	1
6	2	3	1	2
7	3	1	3	2
8	3	2	1	3
9	3	3	2	1

The fiber generated out of these 9 experiments was imaged by a SEM after gold coating the samples so as to avoid charge accumulation. The fiber diameter was obtained from SEM (2500X) image of each sample, from each image fiber diameter was measured at 20 random data points by and these 20 observations were averaged to give mean fiber diameter (Fig 1). The software “Minitab-16” and “SPSS-12” was used in the orthogonal table design and ANOVA analysis respectively. An inbuilt function for Taguchi analysis in Minitab 16 is used to interpret the significance level of each factor on fiber diameter and morphology of obtained fibers. The four variables, PEO: PCL, solvent, flow rate and voltage were set as factors and mean fiber diameter obtained from the analysis of SEM image was fed as response variable. The result of range analysis aided in arriving at the most significant parameter of the four thus prioritizing each factor with respect to other in order to gain a better control of the fiber morphology. Minitab 16 was executed to open a generalized excel worksheet in Minitab. The input parameters as per L9 DOE values were fed into the respective cells in column wise order PEO: PCL, Solvent, Flow rate and then followed by Voltage (Table 6). The mean fiber diameter obtained for corresponding experiments were also entered in respective rows.

Table 2.5: Taguchi DOE for PEO: PCL fiber diameter optimization.

Trial	PEO:PCL (3.75% g/ml)	Solvent AA: C (%)	Flow rate (ml/hr)	Voltage (kV)
1	1:1	5:95	0.2	14
2	1:1	10:90	0.25	16
3	1:1	20:80	0.3	18
4	1:2	5:95	0.25	18
5	1:2	10:90	0.3	14
6	1:2	20:80	0.2	16
7	1:3	5:95	0.3	16
8	1:3	10:90	0.2	18
9	1:3	20:80	0.25	14

The following steps were followed to set the parameters for Taguchi analysis:

- 1) Click on the tool **STAT** in the toolbar, **>DOE, >Taguchi, >Create Taguchi design** Following this a popup window appears with different number of levels and factors, off these the **Level of design** was set to **3-Level design**. Click on **Designs** option in the same window and select on **L9** option under **Runs**.
- 2) Again navigate through the following: **STAT>DOE>Taguchi>Analyze Taguchi design**. A new window appears with a box in the left side containing list of all columns, select the column containing the response values one by one. In the same window i.e. **Analyze Taguchi design, Graphs** option is selected to open up with a new popup window, mark on **Signal to Noise ratios** and **Means** option. Click on **Analysis** to mark **Signal to Noise ratios** and **Means** option under **Display response table for**. Under **Options > Signal to Noise ratios** was set as **Nominal is best**.

Fig 2.1: Procedure for Taguchi Analysis by Minitab 16.

The figure illustrates the Minitab 16 interface for performing a Taguchi analysis. The main window shows a worksheet with columns C1-T, C2-T, C8, C9-T, C10, C11, C12, C13, and C14. The 'DOE' menu is open, showing options like Factorial, Response Surface, Mixture, and Taguchi. The 'Taguchi' option is selected, leading to a submenu with 'Create Taguchi Design...', 'Define Custom Taguchi Design...', 'Analyze Taguchi Design...', and 'Predict Taguchi Results...'. Below the main window, several dialog boxes are shown: 'Taguchi Design' (Type of Design: 3-Level Design, Number of factors: 4), 'Analyze Taguchi Design' (Response data are in: Trial 1, Trial 2, Trial 3), 'Taguchi Design - Design' (Runs: 3***, Columns: 4), 'Analyze Taguchi Design - Options' (Signal to Noise Ratio: Nominal is best), 'Analyze Taguchi Design - Analysis' (Display response tables for: Signal to Noise ratios, Means), and 'Analyze Taguchi Design - Graphs' (Generate plots of main effects and interactions in the model for: Signal to Noise ratios, Means).

(3.2.1.2) ANOVA analysis:

ANOVA analysis for the fiber diameter with respect to each parameter is obtained in order to find out any significant variation being brought into effect by individual parameter. This analysis helps in arriving at a conclusion that it is combination of the factors or the individual factor which determines the fiber morphology.

Background. In case 3 treatments are to be compared (A, B, C) then it would require 3 separate *t*-tests (comparing A with B, A with C, and B with C). Similarly for seven treatments we would need 21 separate *t*-tests. This would be time-consuming moreover, it would be inherently flawed because in each *t*-test we a 5% chance of our conclusion being wrong is accepted (when we test for $p = 0.05$). Hence, in 21 tests there is a probability that one test would give us a false result. ANalysis Of Variance (ANOVA) overcomes this problem by enabling to detect significant differences between the treatments *as a whole*. Thus a single test is enough to perceive any differences between the means at our chosen probability level.

Describing a population: practical steps

1. Tabulate the data.
2. Sum the data to obtain Σx , then square this to obtain $(\Sigma x)^2$
3. Calculate the mean, \bar{x}
4. Square each data value and sum the squares to obtain Σx^2
5. Calculate $\Sigma d^2 = \Sigma x^2 - \frac{(\Sigma x)^2}{n}$
6. *Estimate* the variance of the population (σ^2) as:

$$\frac{\Sigma d^2}{n - 1}$$

7. Find the *estimated* standard deviation of the population (σ) = square root of the variance.
8. Calculate the *estimated* standard error (SE) of the mean (σ_n) = σ / \sqrt{n}

(3.3) Fabrication of SDVG with Fucoïdan loaded luminal surface:

The optimized operating and solution parameters which were established by Taguchi analysis was employed as such in this fabrication process and also in the experiments carried out further. To form a Fucoïdan loaded PEO: PCL layer the drug Fucoïdan had to be dispersed in PEO:PCL polymer blend. On considering the insolubility of Fucoïdan in chloroform a specific order of component addition was followed to obtain a stable and homogenous Fucoïdan-PEO-PCL blend. A stipulated quantity of Fucoïdan (100mg) is supplemented to 20ml of acetic acid and subjected to constant stirring in a magnetic stirrer for 10mins. After obtaining the uniformity in dispersion of Fucoïdan 125mg of PEO is added to the mixture and stirred for 30 min's. This is followed by addition of 250mg of PCL and 80ml of Chloroform to the mixture and then the resultant solution is agitated for 3 hrs to obtain stability and uniformity in dispersion of each of the mixture components throughout the solution.

To form a Fucoïdan loaded luminal surface of SDVG the Fucoïdan-PEO-PCL blend is first electro-sprayed over rotating mandrel collector with following operating and parameters: (1)Voltage: 22Kv (2) Collector distance of 12 cm and Flow rate: 0.4 ml/hr. The initial preliminary experiments to attain such a graft suffered from a problem in retrieval of the graft from the rotating mandrel collector after the fiber is deposited. This happens because the Fucoïdan loaded layer which is deposited first arrives at the collector in a semisolid phase and solidifies over the collector in course of time leading to tight attachment of the Fucoïdan loaded layer on the collector. In order to overcome this complication a thin PEO/PCL polymer nanofiberous mat is deposited over the collector prior to electro-spraying of Fucoïdan laded polymer blend. The PEO: PCL nano-fiber mat was deposited by employing the same solution and operating parameter as obtained from the Taguchi optimization process. The PEO:PCL nanofiberous mat deposited first over the collector solidifies almost to completion before its arrival at the collector hence does not attach to the collector firmly and thus the SDVG fabricated at the end can be drawn out of the collector easily. Over this nanofiberous mat now a Fcoïdan loaded PEO: PCL is electro-sprayed with operating parameters: (1) Voltage: 22Kv (2) Collector distance of 12 cm and Flow rate: 0.4 ml/hr.

Once the luminal surface is fabricated a thicker layer of uniform and oriented PEO: PCL nano-fiber is deposited over the collector. To form a SDVG with a thickness of 0.250mm the PEO: PCL solution is electrospun at a Flow rate of 0.3 ml/hr for 3 hrs. Other operating parameters were Voltage: 16kV, Collector distance: 14cm and temperature and humidity being maintained as 20 °C and 55% respectively. On completion of the sequence to fiber deposition the SDVG thus formed over the collector is retrieved from the collector carefully and kept in a dessicator for about 4 hrs to air dry. The same construct was then taken forward for SEM analysis later on to confirm uniformity in the SDVG fabricated.

(3.4) Fabrication of Fucoïdan loaded bi-layered vascular graft like conduit:

The optimized value for the uniform and oriented nano-fibers from the above analysis was employed for further graft fabrication. The SDVG sought after in this work is a bi-layered graft with an intermediate Fucoïdan loaded layer. In order to fabricate a SDVG the diameter of the rotating mandrel collector fixed as 5mm. The collector was coupled with the axel of an motor whose rpm could be well regulated to desired value. The polymer solution that forms a drop at the tip of the spinneret experience a extension force due to charge repulsion and this is counteracted by the surface energy of the droplet. On increasing the voltage applied to certain threshold value the charge accumulated in the droplet is sufficient enough to overcome the surface energy and thus the polymer solution forms a jet. This polymer jet undergoes thinning and solidification during its course towards the collector and finally gets deposited over it as it is grounded.

The first layer deposited form the innermost layer of the graft, a solution of 1:2 PEO: PCL polymer proportion in chloroform and acetic acid (80:20) solvent system is used to form a uniform and oriented nanofiberous first layer. After time lapse of 5 min's, a Fucoïdan loaded intermediate layer is fabricated by electro spraying a solution of PEO/PCL-Fucoïdan in chloroform and acetic acid (80:20). About 0.15g of Fucoïdan, 0.125g of PEO and 0.250g of PCL was mixed in 2ml of acetic acid and 8ml of chloroform for 4 hours to obtain a homogenous and stable solution. Then the construct was allowed to stand for another 5 min's.

This is followed by electrospinning 3ml of PEO/PCL polymer solution with same polymer composition and operating parameters as that of the first layer. The operating parameters for the first layer and the second layer being 14kV voltage, tip-collector distance of 14cm, rpm of 1500 and flow rate of 0.3ml/hr. Similarly the operating parameter for the intermediate layer was also same except voltage which was set to be 20kV. Temperature and humidity were maintained as 20 °C and 55% respectively.

(3.5) Study of interface and dimensional uniformity:

The bi-layered conduit fabricated over the base of aluminum foil removed from the collector, the polymer conduit is then cut crosssectionally with good precision. The sections obtained were then examined under SEM for the uniformity in diameter along the length of the graft. The thickness of each layer (first layer , intermediate layer, and second layer) is measured by mounting the sections over a 0.1mm*0.1mm gridded colony counter glass slide and observing then under optical microscope. The graft was examined at three predestined points along the length i.e. at 2cm, 4cm and 6cm.

(3.6) FTIR characterization of Fucoidan loaded nanofibers:

In order to characterize the mode of drug inculcation in PEO: PCL nanofiber matrix a FTIR analysis of PEO/PCL, Fucoidan and Fucoidan inculcated PEO/PCL was carried out. A comparative IR absorption of PEO/PCL, Fucoidan and Fucoidan inculcated PEO/PCL in 4000cm^{-1} to 800cm^{-1} range was used as the basis to identify any new group formation between PEO/PCL and fiber matrix. Thus this study characterizes the mode of Fucoidan immobilization in PEO/PCL.

(3.7) Study of Fucoidan release profile from the bi-layered:

The bi-layered fucoidan loaded conduit is cut cross-sectionally into 8 equal pieces, each weighing around $10 \pm 0.5\text{mg}$. These segments were then placed, in a 12 well tissue culture plate (triplicate) and immersed in 2ml of 33mM phosphate buffer saline (PBS, pH 7.4) solution at 37°C . The experiment set was mounted over a gel tracker to simulate a dynamic

release medium. At pre-determined time intervals, 1ml of release medium was collected and replaced with an equal volume of fresh buffer medium. The amount of Fucoïdan in the reservoir PBS was estimated by phenol-sulfuric acid method (absorbance at 330 nm which is A_{\max} for L-Fucose). To bring the absorbance values in the range of the standard graph, to each 1ml of release medium sampled 1ml of PBS is added. The UV-Visible spectrometer was baseline corrected with 33Mm PBS and the absorbance for the sampled out release medium was measure with PBS as blank. The uniformity in the distribution of the drug (Fucoïdan) in the nano-fiberous construct is established by the analysis of the total Fucoïdan released by 8 equal pieces of the same conduit into PBS over a prolonged period of time.

With an aim of providing a good absorbance for the Fucoïdan concentration in the release medium, the intermediate layer of the bi-layered graft was loaded with 100mg(upper limit) of Fucoïdan, in spite of the know intuition that such high levels can foster a change in fiber morphology. A small disparity in the total Fucoïdan added to the polymer blend and the total Fucoïdan inculcated in the vascular conduit was observed (0.2mg) which was ascribed to the following:

- 1) Loss of the small portion of fiber in the electrospinning process and graft retrieval from the collector.
- 2) The Fucoïdan estimation is based on the L-Fucose content rather than the Fucoïdan itself.

Chapter 4

Results and discussion

(4.1) Extraction and Characterization of Fucoidan:

(4.1.1) Extraction of Fucoidan from brown seaweed *Sargassum weitti*:

The anticoagulant activity of the purified Fucoidan was examined by activated partial thromboplastin time (APTT) assay. Fucoidan significantly prolonged the clotting time; 5 µg of Fucoidan delayed the blood clotting time approximately by 7 times than untreated control. The anticoagulant activity of the purified Fucoidan increased almost linearly with increasing concentration (0.1, 0.2, 1.0, 2.0, 3.0, 5.0 µg) of the Fucoidan (Fig.4.1). 1microgram/ml standard solution of extracted Fucoidan was prepared and clotting time was noted for 0.1 ml, 0.2,1,2,3,5 ml of the solution.

Table 4.1: Response of clotting time with change in Fucoidan concentration.

Concentration of Fucoidan (1 microg/ml)	Clotting time – 1 (seconds)	Clotting time – 2 (seconds)
0	35	32
0.1	55	58
0.2	88	82
1	150	161
2	172	174
3	224	231
5	280	274

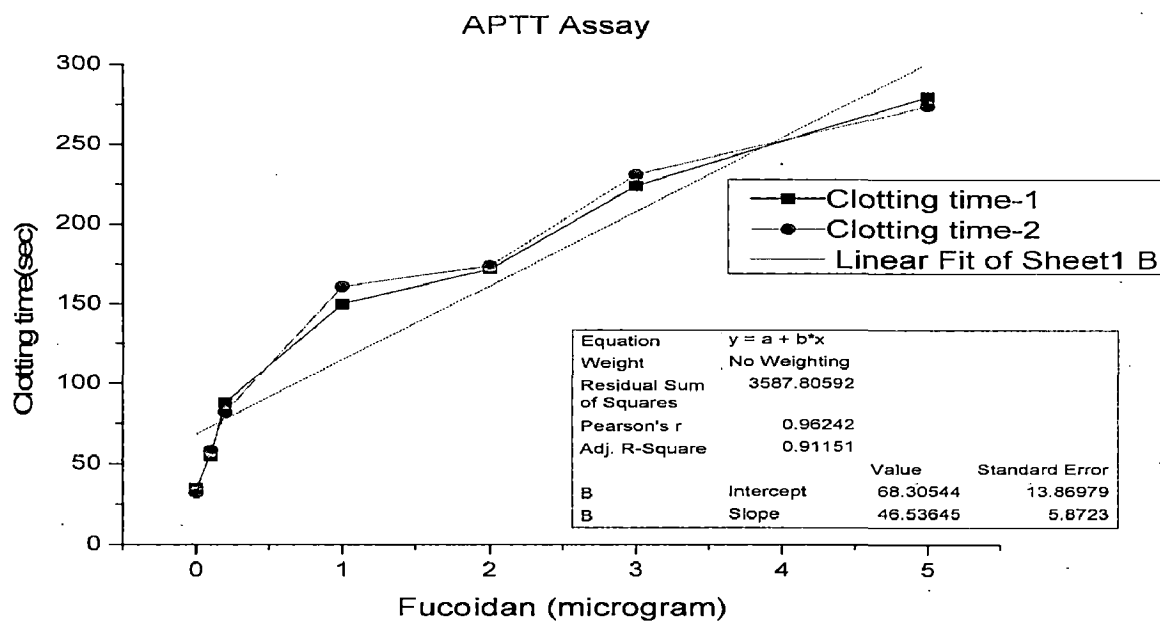


Fig 4.1 : Plot of Clotting time with amount of Fucoidan (micrograms), almost a linear raise in clotting time is observed with increase in quantity of Fucoidan. Implying that the major component of the fraction extracted is Fucoidan.

(4.1.2) FTIR confirmation and characterization for extracted Fucoidan :

A FTIR analysis of the crude Fucoidan extracted from *Sargassum wightii* was carried out for confirmation of the presence of Fucoidan. The IR spectrum showed typical absorption bands of Fucoidans. Absorption at 1322 and 1103 cm^{-1} signifies the presence of sulfate groups in the mixture (i.e. sulfate group attached to the poly-saccharide unit). The 1103 cm^{-1} absorbance was reported in a previous study of Fucoidan and was suggested to be due to sulfate groups at the axial C-4 position. Sulfate groups at the equatorial C-2 and C-3 positions were reported to give a small shoulder of absorption at 1190 cm^{-1} , and there is such a shoulder in the Fucoidan extract at 1160 cm^{-1} . The Fucoidan contained a hydroxy group band at 3430 cm^{-1} as well as a carbonyl band at 1629 cm^{-1} . Small disparities in the IR spectra obtained in different reports can be due to a number of factors including sample handling and the extraction processes used. While IR spectroscopy confirmed key signature features of Fucoidans in the *Sargassum wightii* isolated, comparative analysis of IR spectra

obtained in this work for commercial Fucoïdan and the Fucoïdan extract clearly supports the identification of extracted polysaccharide as a Fucoïdan (Fig 4.2).

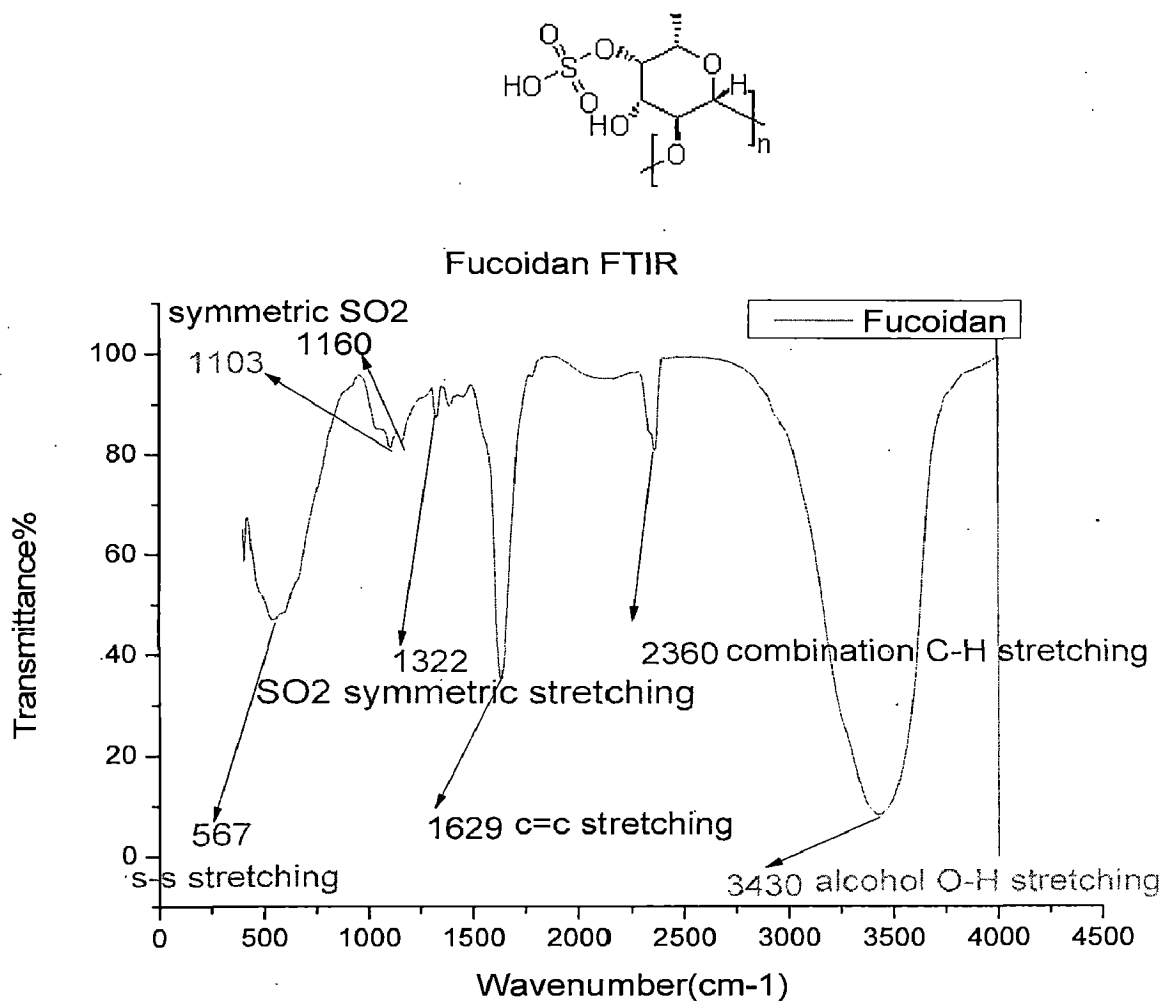


Fig 4.2: FTIR analysis of the fraction extracted and its correspondence to the groups present in Fucoïdan.

(4.1.3) Estimation of Fucoïdan extracted from *Sargassum weitti*.

The L-Fucose solutions with a uniform gradient in concentration of L-Fucose were taken for phenol-sulfuric acid assay. The absorbance of each solution at 330nm was measured and tabulated thereby generating a standard graph for L-Fucose sugar. As the major content of Fucoïdan is L-Fucose an estimation of L-Fucose will give an approximate estimation of Fucoïdan hence this standard is used to estimate the amount of Fucoïdan in further experiments.

Table 4.2: Absorbance with change in concentration of L-Fucose.

Fucose (micro-gram)	OD-1	OD-2	OD at 330nm.
200	0.15	0.18	0.16
300	0.34	0.26	0.30
400	0.58	0.46	0.53
500	0.82	0.94	0.88
600	1.52	1.40	1.46

The absorbance of the sample (crude Fucoidan fraction from mild acid-ethanol extraction process) of 4ml in volume was found to be 0.62 which corresponds to 460micro-gram of L-Fucose (i.e. approximately 370 micro-grams of Fucoidan in 4ml). The total volume of the extract was 45ml, hence about 4070 micro-grams (i.e. 4.07g) of Fucoidan was extracted from 100 grams of dry *Sargassum wightii* (which is 4% by weight of the biomass).

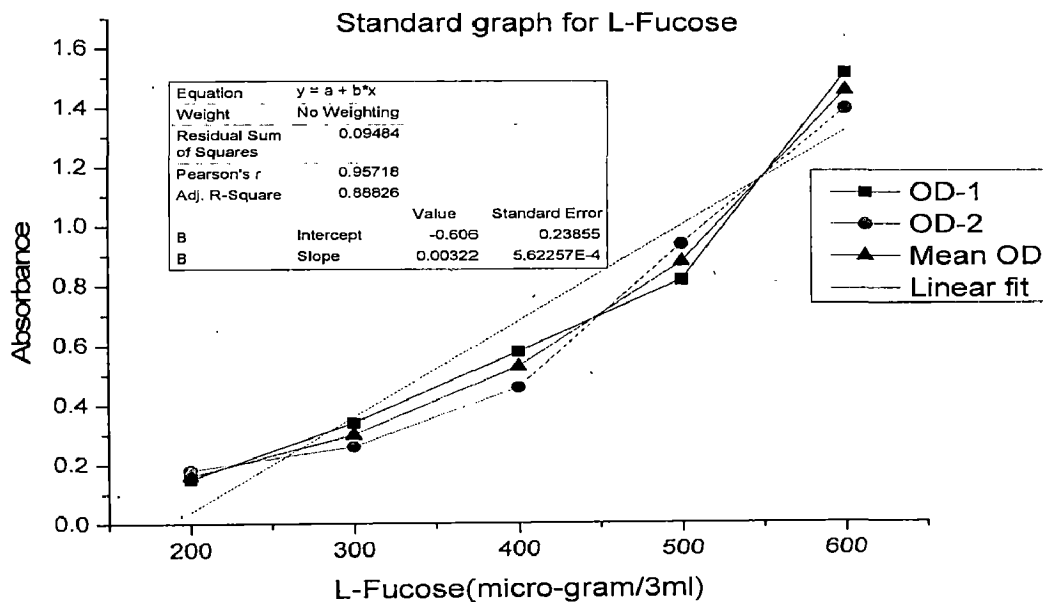


Fig 4.3: Plot of absorbance with increase in concentration of Fucoidan, this standard graph was used to interpret the Fucoidan concentration in the fraction extracted.

4.2 Fiber diameter and Morphology:

The study of the SEM images of the PEO-PCL nanofibers helps perceiving the effect of each polymer and solvent individually on the fiber morphology and orientation. Fiber orientation plays an important role in the as it determines to a great extent the motility and endotheliasation of the nanofiber scaffold. The high rpm of the collector ensures the orientation of the polymer nanofiber depositing over the collector. An aluminium foil conduit of 5mm inner diameter was employed as collector for preliminary study. All the nanofibers produced by the possible combination had two things in common, first being that the fibers were well oriented, and the other one being that the fiber surface has roughness/irregularity (Fig 4.4).

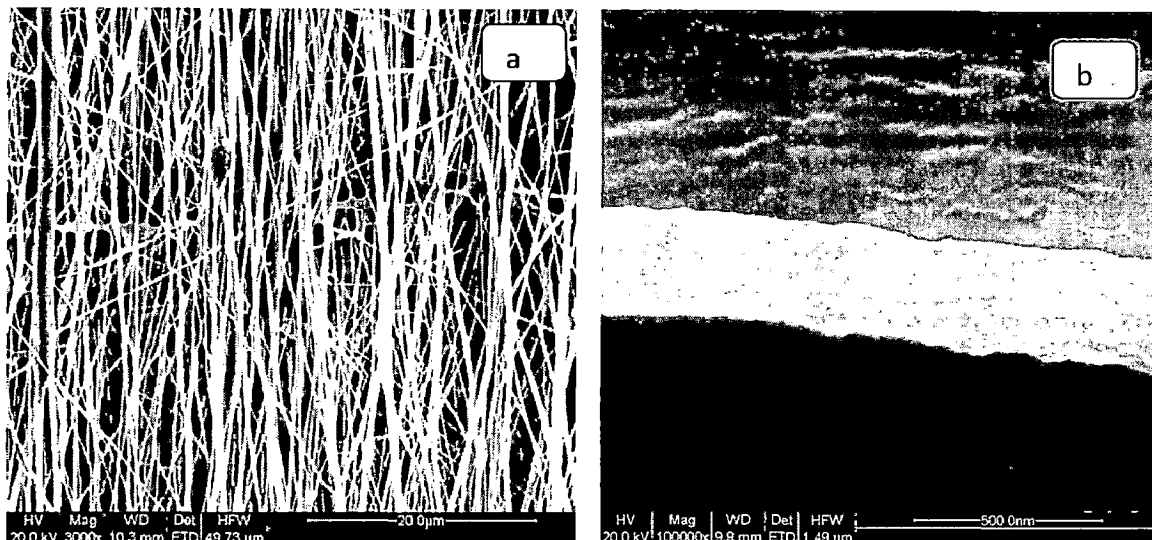


Fig 4.4: SEM images of PEO-PCL polymer nanofibers with composition as 20% acetic acid and 80% chloroform solvent system and 1:2 PEO:PCL 20ml (g/20ml) of PEO-PCL.(a) Orientation of the fibers (b) surface morphology of the fiber.

The fiber surface roughness improves the attachment of the EC's and SMC's over them and thus helps in improving the chances of improved patency of the nano-fiber scaffold. The roughness is imparted to the nano-fiber to a large extent by the high proportion of chloroform employed i.e. 90%, 80% and 95% and this trend could be

easily conceived from the nanofiber surface obtained for corresponding solvent system.

This arises because of the fact that chloroform being less volatile relatively to that of acetic acid moves out of the polymer fiber in the latter phase of polymer stream solidification process thereby rendering roughness to the fiber surface. Other significant observation is that with increase in proportion of PEO:PCL produced beaded and non-oriented nano-fibers this could be explained by the contrast in SEM images between two solution compositions 1:1 and 1:3 PEO:PCL in 10% acetic acid and 90% chloroform (Fig 4.5). This is an outcome of the differences in two properties one is crystallinity and the other being the molecular weight. In PEO and PCL polymer blend, PEO being semi-crystalline has an inherent tendency to remain as randomly oriented molecular chains and hence it favors the bead formation rather than the fiber formation (Fig 4.5 (b)).

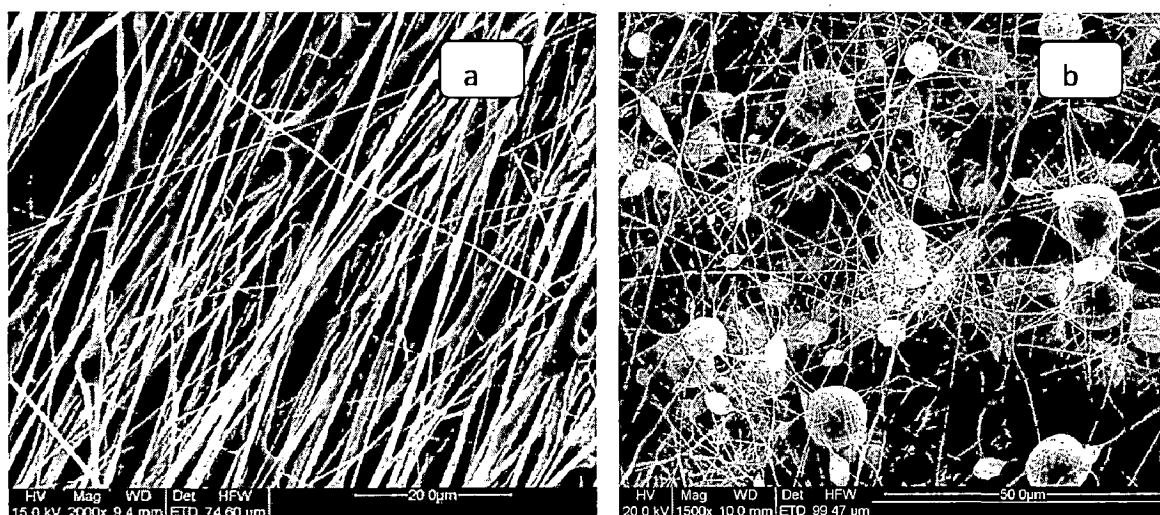


Fig 4.5: SEM images showing the fiber morphology variation with respect to PEO:PCL composition. (a) 1:2 PEO:PCL in 20ml of (10% acetic acid and 90% chloroform), (b) 1:1 PEO:PCL in 20ml of (10% acetic acid and 90% chloroform).

Thus higher the proportion of the PEO higher will be tendency to produce beads. The other factor i.e. discrepancy in molecular weight of PCL and PEO also contributes to the bead formation though to a smaller extent than the crystallinity.

Molecular weight signifies the polymer chain length, larger the polymer length higher will be the tendency to form intra-chain bonding, this kind of intra-chain interaction improves the chances of a polymer to extrude as a fiber rather than a bead. Hence PEO which has a lower molecular weight than PCL produces beads.

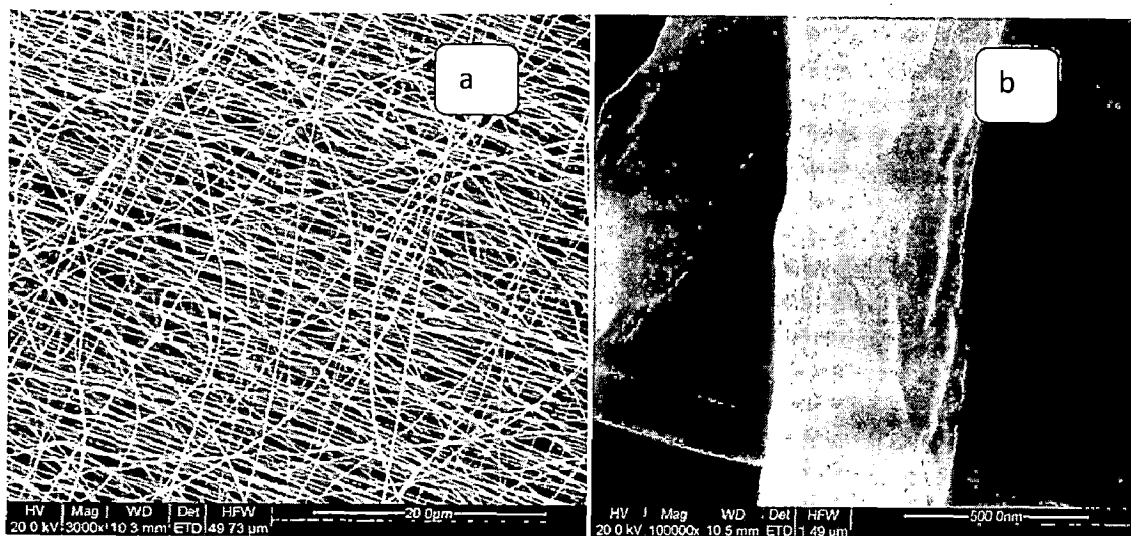


Fig 4.6: PEO-PCL nano-fibers prepared by electrospinning 1:2 wt% in 20ml solvent of 20% acetic acid and 80% chloroform (a) at lower magnification (b) at higher magnification.

Table 4.3: L9 Taguchi DOE with fiber diameter response for each corresponding trial.

Trial	PEO:PCL* (3.75% g/ml)	Solvent AA: C** (%)	Flow rate (ml/hr)	Voltage (kV)	Mean Fiber diameter (nm)
1	1:1	5:95	0.2	14	564.71 ±215 nm
2	1:1	10:90	0.25	16	877.70±413 nm
3	1:1	20:80	0.3	18	249.78 ±54 nm
4	1:2	5:95	0.25	18	291.66 ±53nm
5	1:2	10:90	0.3	14	287.86 ±37 nm
6	1:2	20:80	0.2	16	381.19±124 nm
7	1:3	5:95	0.3	16	577 ±139 nm
8	1:3	10:90	0.2	18	477.37 ±106nm
9	1:3	20:80	0.25	14	758.79 ±177 nm

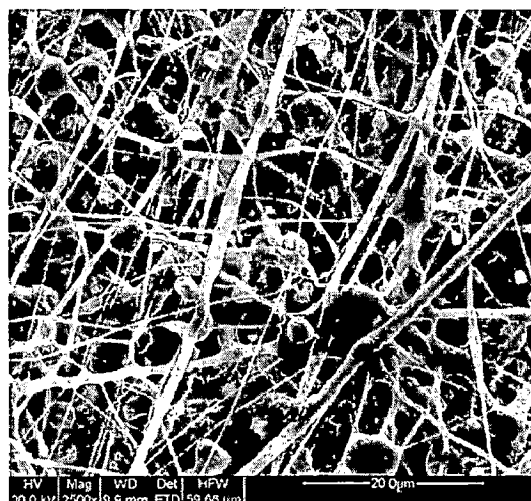
* PEO/PCL – poly-ethylene oxide, ** AA:C – Acetic acid : Chloroform

As an oriented nano-fiber with almost no beads is the most preferable morphology for patency of SMC's and EC's the polymer solution with lower proportion of PEO is favorable for nano-fiber production. The study of morphology of the nano-fibers gives a composition of the polymer and solvent system that is most suitable for the desired fiber morphology (Fig 4.6). The most favorable one being PEO:PCL polymer solution with 1:2 wt% in 20 ml of 20% acetic acid and 80% chloroform solvent system.

Table 4.3: Fiber diameter and morphology for L9 Taguchi DOE.



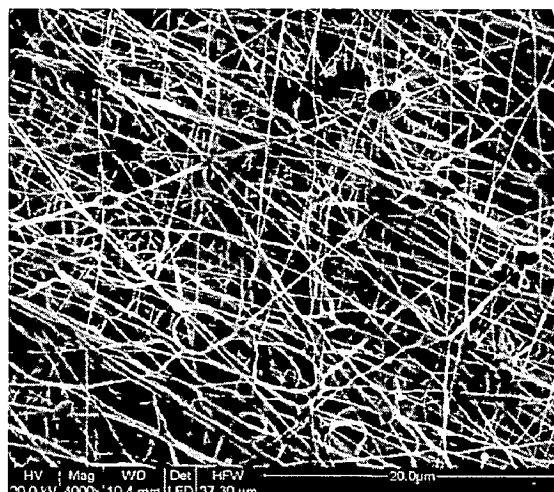
Trial: 1, PEO: PCL proportion: 1:1,
Chloroform: acetic acid proportion: 5:95,
Voltage: 14 kV, Flow rate: 0.2 ml/hr
Fiber diameter: 564.71 ± 215 nm



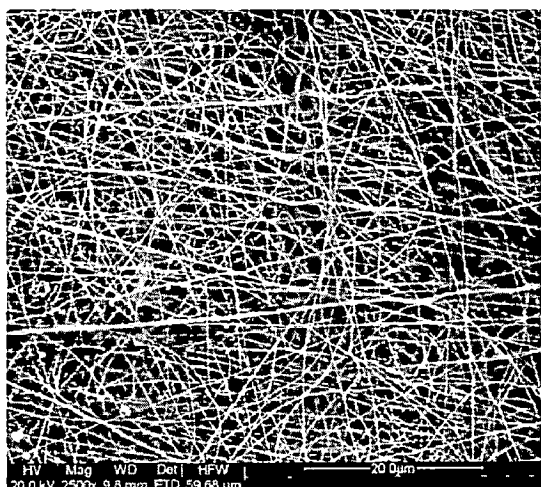
Trial: 2, PEO: PCL proportion: 1:1,
Chloroform: acetic acid proportion: 10:90,
Voltage: 16 kV, Flow rate: 0.25 ml/hr
Fiber diameter: 877.70 ± 413 nm



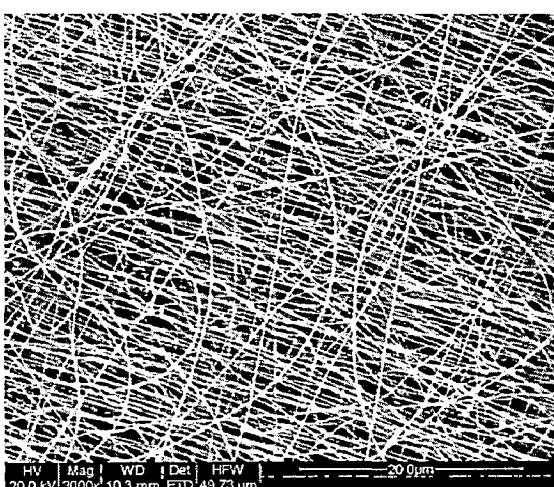
Trial: 3, PEO: PCL proportion: 1:1,
 Chloroform: acetic acid proportion: 20:80,
 Voltage: 18 kV, Flow rate: 0.3 ml/hr
 Fiber diameter: 249.78 ± 54 nm



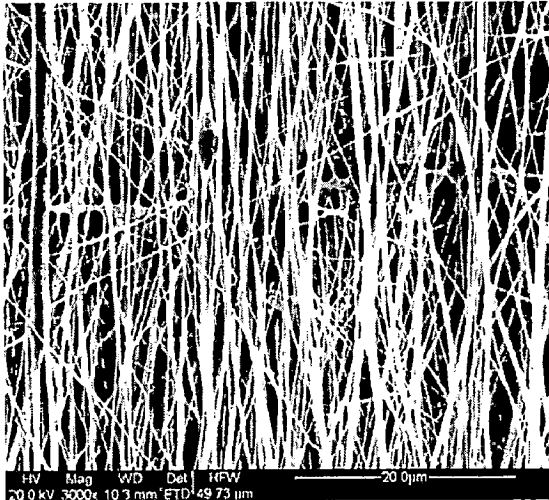
Trial: 4, PEO: PCL proportion: 1:2,
 Chloroform: acetic acid proportion: 5:95,
 Voltage: 18 kV, Flow rate: 0.25 ml/hr
 Fiber diameter: 291.66 ± 53.74 nm



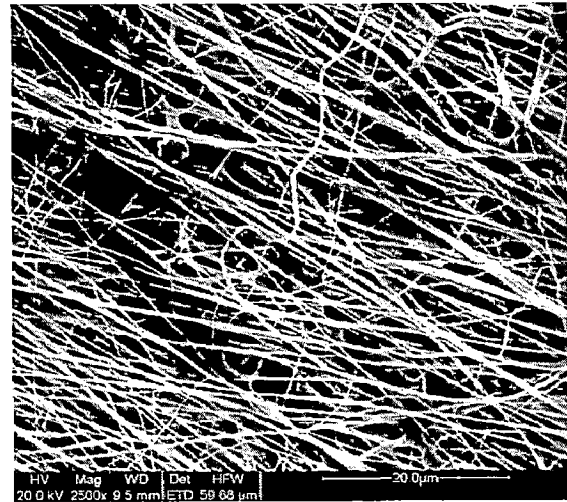
Trial: 5, PEO: PCL proportion: 1:2,
 Chloroform: acetic acid proportion: 10:90,
 Voltage: 14 kV, Flow rate: 0.3 ml/hr
 Fiber diameter: 287.86 ± 37 nm



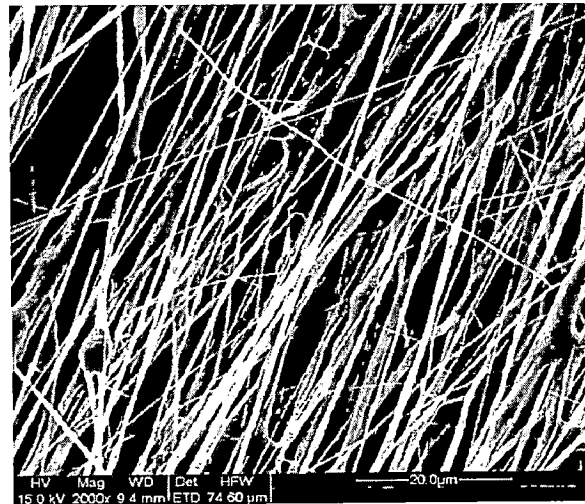
Trial: 6, PEO:PCL proportion: 1:2,
 Chloroform: acetic acid proportion: 20:80,
 Voltage: 16 kV, Flow rate: 0.2 ml/hr
 Fiber diameter: 381.19 ± 124 nm



Trial: 7, PEO: PCL proportion: 1:3,
 Chloroform: acetic acid proportion: 5:95,
 Voltage: 16 kV, Flow rate: 0.3 ml/hr
 Fiber diameter: 577 ± 139 nm



Trial: 8, PEO: PCL proportion: 1:3,
 Chloroform: acetic acid proportion: 10:90
 Voltage: 18 kV, Flow rate: 0.2 ml/hr
 Fiber diameter: 477.37 ± 106 nm



Trial: 9, PEO: PCL proportion: 1:3,
 Chloroform: acetic acid proportion: 80:20,
 Voltage: 14 kV, Flow rate: 0.25 ml/hr
 Fiber diameter: 758.79 ± 177 nm

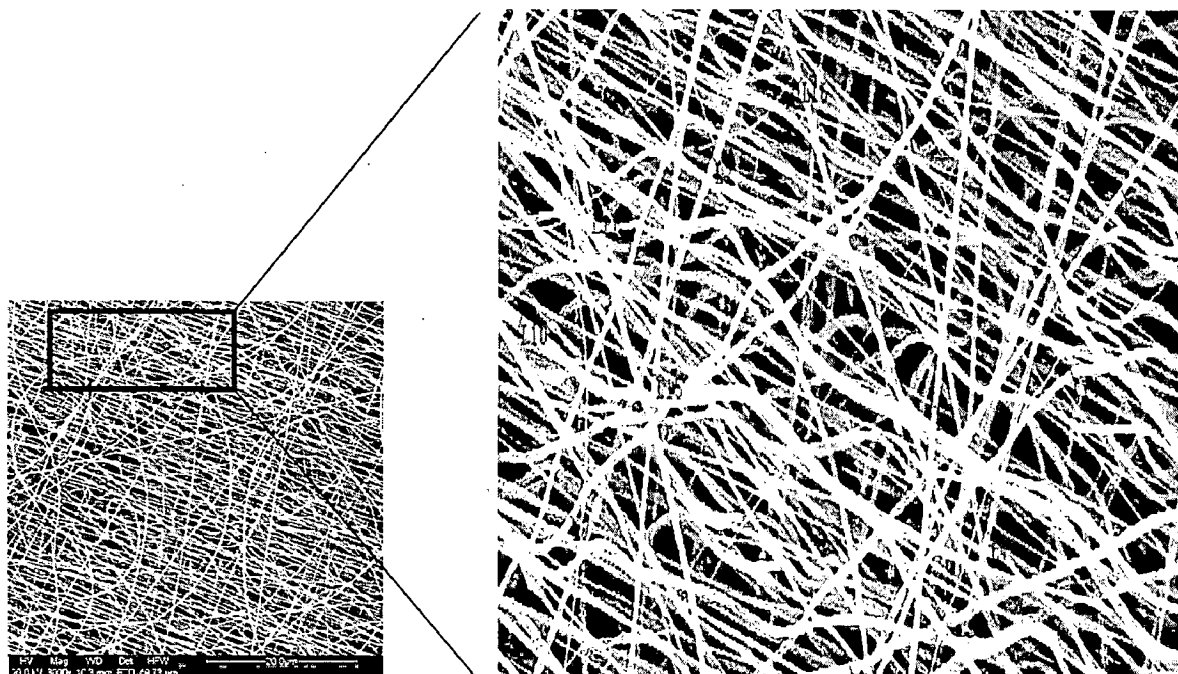


Fig 4.7: Fiber diameter measurement by Materials Plus 12.

(4.2.1) Range analysis by Taguchi DOE:

Range analysis was carried out in order to know the significance level of each operating factor on the fiber morphology and fiber diameter. Table represents the statistical analysis of effect of different factors on nanofiber diameter. The K value for each level of a parameter was the average of three values shown in Table 1 and the range value for each factor was the difference between the maximal and minimal value of the three levels. The square of deviation (s) of three levels for each factor was also determined. On the basis of the results of the range analysis and the square of deviation, the significance level was determined to be as follows: Voltage, PEO:PCL proportion, Flow rate and then Solvent proportion.

Output Sheet:

Taguchi Orthogonal Array Design
 L9(3**4)
 Factors: 4
 Runs: 9
 Columns of L9(3**4) Array

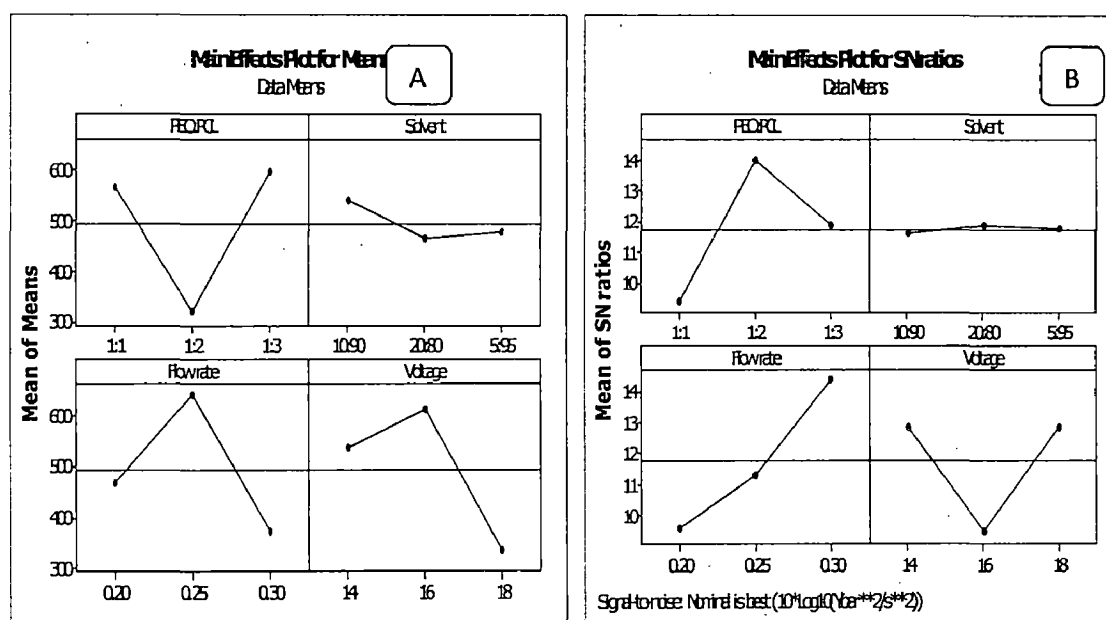
1 2 3 4

Table I: Response table for Means:

Level	PEO:PCL	Solvent	Flow rate	Voltage
K1	564.1	541.6	468.4	537.1
K2	320	463.3	642.7	612.0
K3	598.4	477.8	371.6	333.6
Delta	278.1	78.4	271.2	278.4
Rank	2	4	3	1

Table II: Response Table for Signal to Noise Ratios

Level	PEO:PCL	Solvent	Flowrate	Voltage
1	9.378	11.613	9.580	12.861
2	13.993	11.849	11.288	9.514
3	11.875	11.785	14.378	12.872
Delta	4.614	0.236	4.798	3.358
Rank	2	4	1	3

Nominal is best - ($10 \cdot \log_{10}(\bar{Y}^2/s^2)$)**Fig 4.8: Main effects for (A) Means and (B) S/N ratio.**

(4.2.2) Analysis of variance for fiber diameter with respect to each parameter:

The sum of squares of deviation (SS), degree of freedom (DF), and mean squared deviation (MS) of fiber diameter and beads percent were determined and summarized in Table III. The F value of a factor is the ratio of the MS value of the factor to that of error line. Through comparing the obtained F value with the theoretical one of specific level and DF, the significance level can be determined for each factor. As shown in Table the F value for all the parameters taken into consideration are less than the standard value of 5.1 hence four parameters do not give raise to significant level of difference in fiber diameter with respect to single parameter into consideration. Thus it is the combination of parameters that bring in wide variation in fiber diameter rather than single parameter determining it solely.

From the range analysis in Taguchi optimization method it was inferred that Voltage had maximum level of significance over the fiber diameter then followed by PEO: PCL, Flow rate and solvent system. The analysis of variance analysis aided in arriving at a conclusion that none of the four parameters had an individualistic effect over the fiber diameter.

Table III: One-way ANOVA: Trail 2 versus PEO: PCL Solvent Flow rate Voltage

Source	Degree of Freedom	Sum of Squares	Mean Sum of Squares	F Value	P Value
Solvent	2	12211	6106	0.10	0.908
PEO:PCL	2	141818	70909	1.75	0.252
Flow rate	2	112439	56220	1.24	0.355
Voltage	2	118795	59397	1.34	0.331

Step by step ANOVA for PEO: PCL proportion's effect on fiber diameter.

Table IV: ANOVA table for nanofiber diameter:

	PEO:PCL PROPORTION			
Replicate	1:1	1:2	1:3	Row totals
1	564.71	291.66	577	1433.37
2	877.70	287.86	477.37	1642.93
3	249.78	381.19	758.79	1389.76
\bar{x}	1692.19	960.71	1813.16	4466.06 (call this GT)
N	3	3	3	
\bar{x}	564.06	320.23	604.38	
δx^2	1151644.72	313234.93	1136573.381	2601453.03 (call this A)
$\frac{(\sum x)^2}{n}$	954502.33	307654.56	1095849.72	2358006.6 (call this B)
δd^2	197142.39	5435.37	40723.661	243446.43 (A - B)
$\delta^2 (= \delta d^2 / n-1)$	98571.195	2717.685	20361.83	

$$D = (\text{Grand total})^2 \div \text{total observations} = 19945710.27 \div 9 = 2216190.03$$

$$\text{Total sum of squares (S of S)} = A - D = 385263.44$$

$$\text{Between-treatments S of S} = B - D = 141818.61$$

R

Source of variance	Sum of squares (S of S)	Degrees of freedom *	Mean square (= S of S \div df)
Between treatments	141818.61	$u - 1 (=2)^*$	70909.305
Residual	243446.43	$u(v-1) (=6)^*$	40574.405
Total	385263.44	$(uv)-1 (=8)^*$	48157.93

$$\text{S of S} = A - B = 243446.43$$

[* For u treatments (3 in our case) and v replicates (3 in our case); the total df is one fewer than the total number of data values in the table (9 values in our case)]

F = Between treatments mean square / Residual mean square = 1.75

The tabulated value of F ($p = 0.05$) where u is df of between treatments mean square (2) and v is df of residual mean square (6) is 5.1. Our calculated F value does not exceed this ($F = 1.75$). Hence there is no significant difference between treatments.

(4.2.3) Regression analysis:

Based on above analysis, voltage and PEO/PCL polymer proportion were the most significant

factors that influenced the fiber diameter and beads percent. Statistic software of Minitab 16 was adopted for the regressive analysis. The voltage and PEO/PCL proportion were set as variables, and mean fiber diameter was set as dependant variable. The linear dependence regression equation for fiber diameter was

$$\text{Mean fiber diameter} = 1255 - 49.4 \text{ Voltage} + 0.88 \text{ PEO \%} \dots\dots\dots(4)$$

This regression equation formulates a rough relationship between fiber diameter and two significant operating parameters i.e. voltage and PEO/PCL proportion. This relation provides an idea to scale up or scale down the fiber diameter by varying voltage and PEO/PCL proportion

(4.3) Characterization of Fucoïdan loaded PEO/PCL nanofiber:

(4.3.1) Fiber morphology:

The intermediate layer is formed by electrospaying the Fucoïdan loaded PEO/PCL polymer solution at a higher voltage this results in a dendritic mat of PEO/PCL with beads accompanying it. The dendrite like structure arises because of the higher voltage that is applied and it is required that a higher voltage be applied to electrospin this Fucoïdan loaded PEO/PCL polymer solution to reach the collector because of the

additional solute burden of Fucoïdan. The irregularity in fiber morphology (i.e. diversity in fiber diameter and un-oriented deposition of fiber) is ascribed to the upper limit of Fucoïdan being loaded to the polymer solution. The Fucoïdan being soluble in specific component of PEO/PCL adds up to un-stability of the solution at higher concentration. Hence this factor determines the upper limit of the Fucoïdan that can be loaded in the graft and thus accounting to one of the limitations of the proposed strategy to overcome intimal hyperplasia.

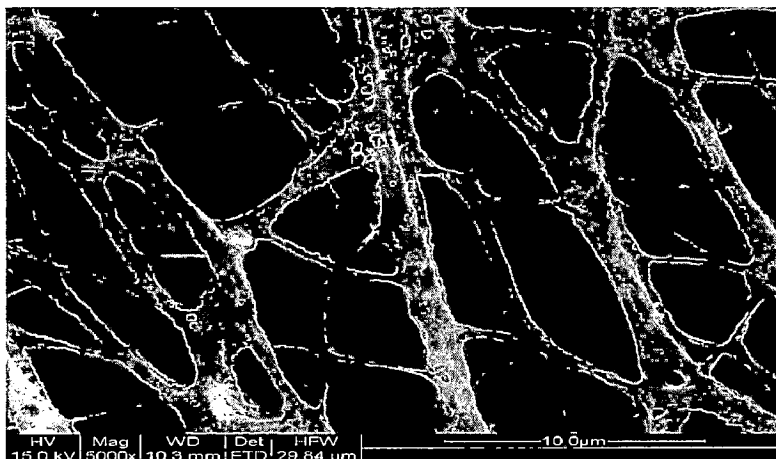


Fig 4.9: Fucoïdan loaded PEO:PCL intermediate layer.

(4.3.2) FTIR characterization of Fucoïdan loaded nanofiber:

The presence of strong and broad peak in the range of 3300-3600 cm^{-1} signifies the presence of large fraction of -OH group that exists in polysaccharide component of Fucoïdan (61). A asymmetric C-H stretch of the methyl and methylene groups at 2948 cm^{-1} is observed accounting for the aliphatic chains in PEO and PCL(61,64). Absorption at 1720 cm^{-1} indicates the presence of ketone in PCL(64). A strong absorption at 1641 cm^{-1} probably arises out of C=C group of PEO(64). Other specific absorption peaks corresponding to di-alkyl sulfones is observed at 1324 cm^{-1} and 1151 cm^{-1} (64) which is probably from the sulfates attached to the polysaccharide, and a typical characteristic absorption pair for a Fucoïdan (sulfated polysaccharide) is observed at 792 cm^{-1} and 1241 cm^{-1} (62,63).

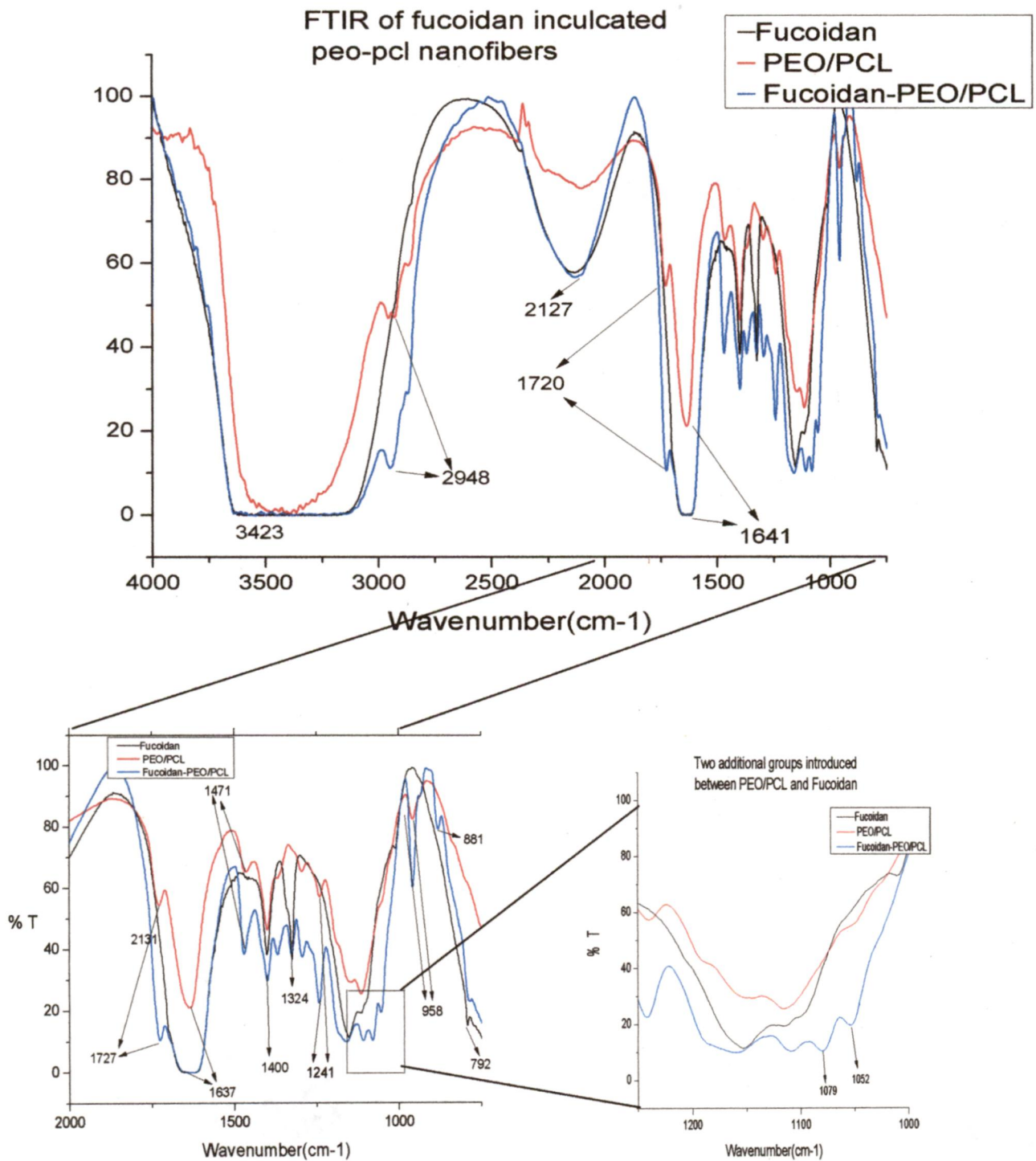


Fig 4.10: FTIR of (1) Pure Fucoidan (2) PEO-PCL nanofibers and (3) Fucoidan loaded PEO-PCL nanofibers.

Appearance of new peaks apart from the linear combination of the two IR spectrums (of Fucoidan and PEO/PCL) in Fucoidan loaded PEO/PCL IR spectrum dictates the chemical linkage between the components of the mixture. Hence, the two new peaks in IR spectrum of Fucoidan loaded PEO/PCL, one at 1052cm^{-1} and the other at 1079cm^{-1} account for sulfoxide (sulfate esters) and C=O of anhydrogalactose respectively. As there is no significant change in FTIR peaks of either PEO:PCL or the Fucoidan the new peaks at 1052cm^{-1} 1079cm^{-1} .

(4.4) Bi-layered Fucoidan loaded SDVG:

The conduit like structure fabricated by deposition of PEO/PCL nanofibers over a collector of 5mm diameter is drawn out of the collector with care (Fig 4.11 (a),(b)). The tubular graft is then cut across cross-sectionally with a high grade knife then carried over for interface study and drug release profile study. The cross sectional SEM images of the conduit (Fig 4.12(a),(b)) shows the Fucoidan loaded intermediate layer well merged (fused) into the first and second layer. This ensures the absence of any discernable separation (i.e. clear interface) between the two layers. The absence of interfaces precludes any kind of compromise in mechanical property owing to the bi-layered structure. The severe lag in mechanical property compliance of most bi-layered vascular graft is due to the anisotropy in properties at the interface. But the image of the PEO-PCL conduit prepared shows no such de-lamination at the interface, hence is a suitable candidate for fabrication of vascular graft.

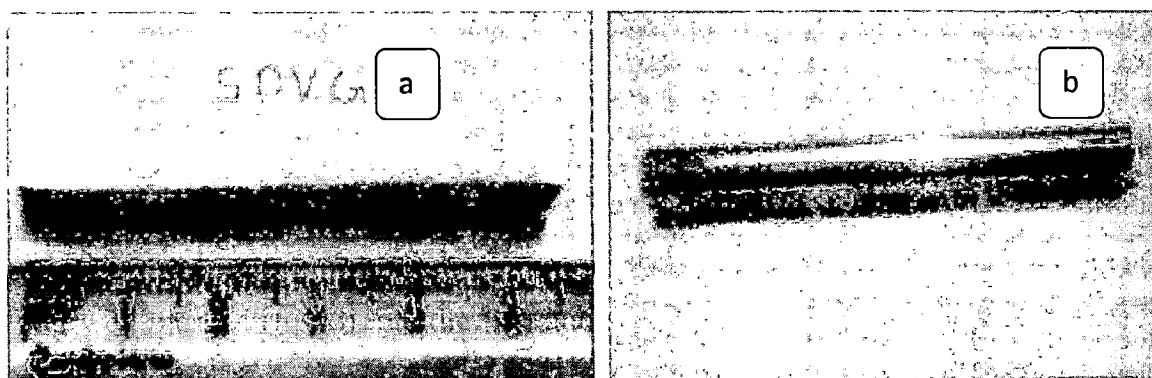


Fig 4.11: The (a) bi-layered nanofibrous SDVG and (b) Aluminum foil collector over which fiber is deposited.

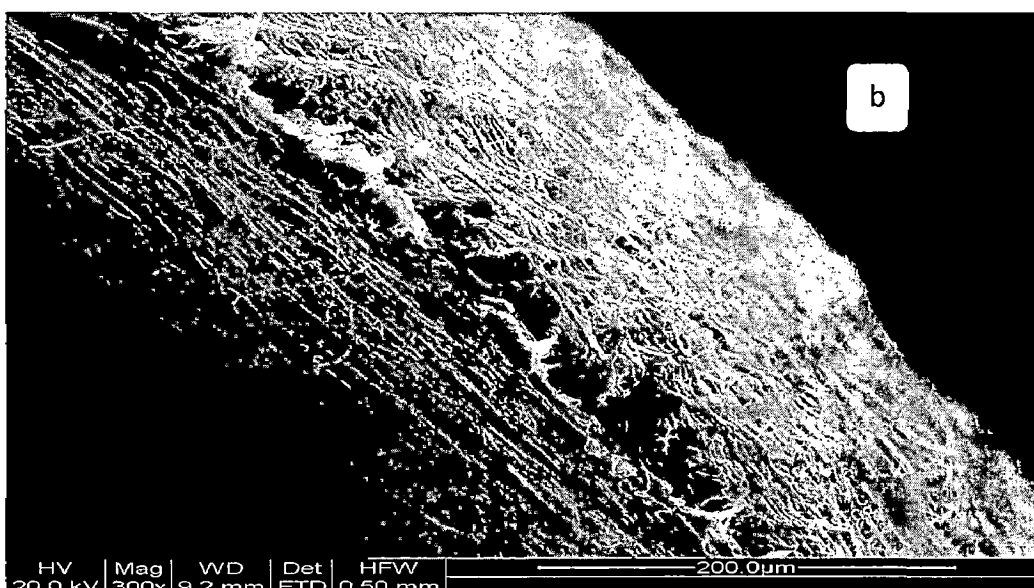
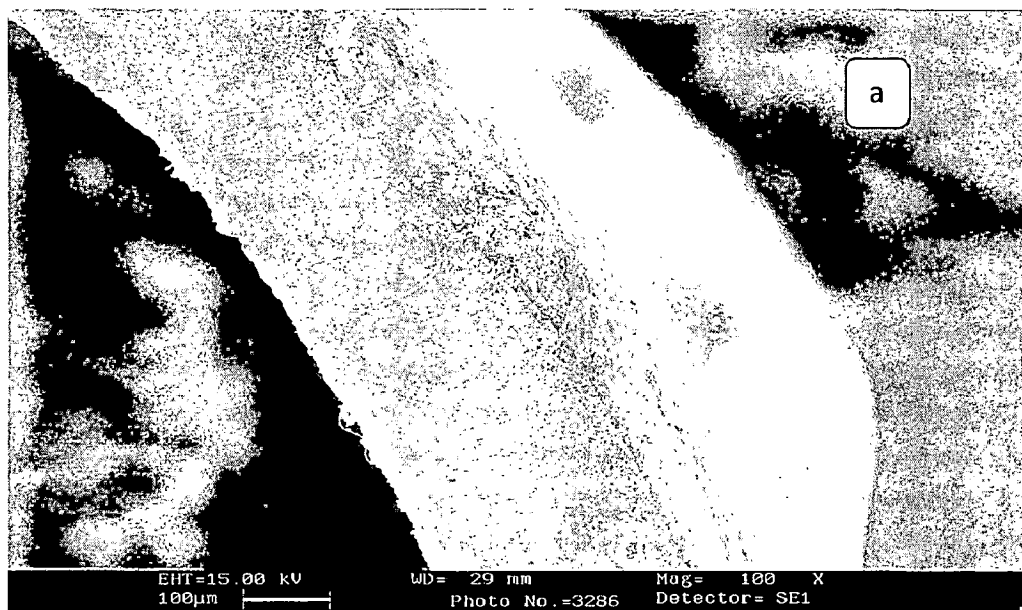


Fig 4.12: Cross sectional view of (a) single layered PEO/PCL nanofibrous graft, (b) bi-layered PEO/PCL conduit with the intermediate being loaded with Fucoidan and sandwiched between the first and second layer.

(4.5) Cross-sectional uniformity of the bi-layered graft prepared:

The graft obtained by above stated procedure is then evaluated for the uniformity in the cross-section of the graft. The conduit like graft was cut along the direction perpendicular to their axis at predestined positions. Three incisions, at 2cm, 4cm and

6 cm were performed and the resultant pieces of graft were then mounted on the stage of optical microscope. A gridded slide used for blood cell count is used as the scale for measuring the cross-sectional diameter and thickness.

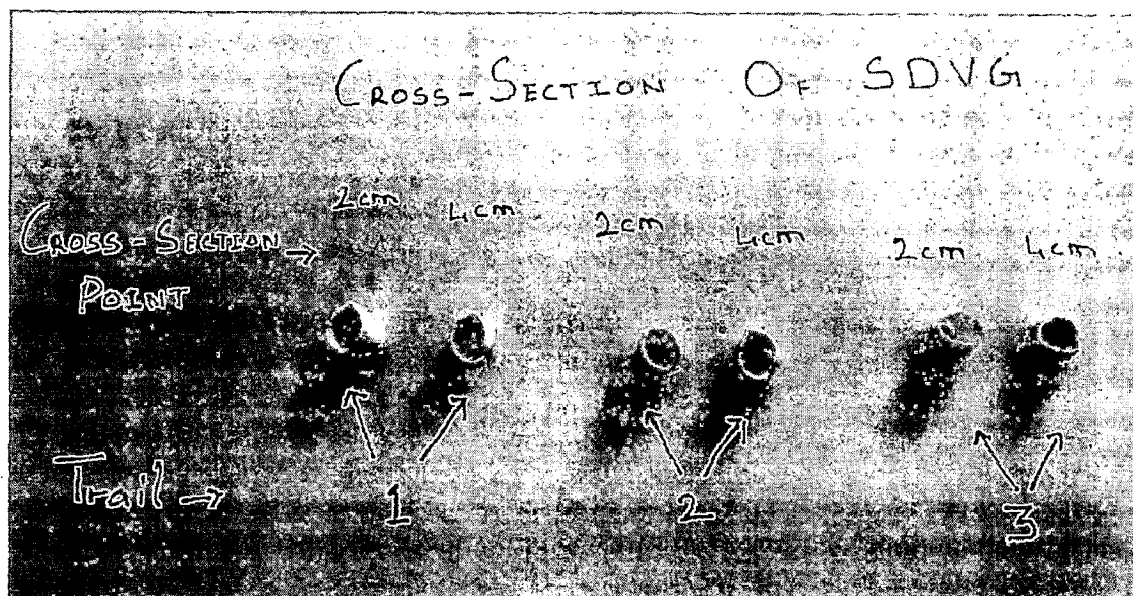


Fig 4.13: Cross-sectional view of 3 Trial SDVG at 4 cm and 2cm distance for each.

Table 4.5: Dimensional uniformity in terms of diameter and thickness of the graft at different points along the graft length.

Target dimension: Inner diameter: 5.5mm Outer diameter: 5.68mm (thickness of 0.16mm)

Graft Trail	Measure point (cm)	Inner Diameter (mm)	Outer diameter (mm)	Thickness (mm)
1	2	5.515	5.680	0.165
	4	5.520	5.678	0.168
	6	5.521	5.682	0.161
2	2	5.518	5.681	0.163
	4	5.522	5.687	0.165
	6	5.519	5.685	0.171
3	2	5.514	5.683	0.169
	4	5.509	5.681	0.172
	6	5.512	5.684	0.172

(4.6) Degradation of PEO/PCL nanofiber:

(4.6.1) DSC analysis:

The PEO/PCL nanofibrous mat obtained is carried over for DSC analysis to study the in vitro degradation rate on incubation in PBS for the respective time interval. From the thermogram obtained it was observed that the PEO composition denoted by its Tg i. 68.4 vanishes in due course of incubation time in PBS. The sample under 4 hour incubation (2) didn't show much deviation from the Tg observed in the initial sample, where as there is considerable difference in Tg of samples incubated for 7 and 12 days, the sample kept in PBS for 12 days almost had only PCL component left in it which was inferred by the lone Tg at 60 C.

The decline in the PEO component with passage of time is because of the higher hydrophilic nature of the PEO component of PEO-PCL blend. The degradation of PEO component also improves the porosity of the nanofibers with also facilitates the infiltration of the SMC into the nanofibrous matrix which would be later predominated by the PCL component of the blend.

(4.7) Fucoidan release profile from bi-layered and mono-layered vascular graft:

Same sampling process and analysis of the sampled volume was followed for both the bi-layered and mono-layered SDVG. The standard graph of L-Fucose is used to estimate the amount of Fucoidan eluted in the release medium i.e. PBS. From 3ml of release medium in each well 1ml is drawn out for Fucoidan estimation.

The Fucose standard graph gives the following relation:

$$\text{Concentration of Fucoidan (microg/ml)} = (\text{Absorbance} + 0.606)/0.0031 \quad (1)$$

Each of the sampled volume is the carried over for Phenol-Sulfuric acid assay and their respective absorbance were measured at 330nm in a UV-Visible spectrophotometer. The blank used for the analysis composed of 1ml PBS, 2ml Sulfuric acid and 0.66ml phenol. The absorbance value were correlated to amount of Fucoidan in the release medium (PBS) by equation (1).

Table 4.6: Amount of Fucoidan released from bi-layered conduit with course of incubation time in PBS.

Sampling time	Absorbance	Fucoidan in testing volume (mg/ml)	Fucoidan in sampled volume (1ml) (mg/ml)	Fucoidan in each release medium (3ml) (mg)	Total release After 480hrs (mg)	Percentage Fucoidan released (%)
2	0.324	0.30	0.60	1.8	9.8	18.36
4	0.479	0.35	0.70	2.2	9.6	22.91
24	0.944	0.50	1.00	3.0	9.7	30.92
48	1.347	0.63	1.26	3.8	9.6	39.58
72	1.595	0.71	1.43	4.3	9.9	43.43
96	1.812	0.78	1.56	4.7	9.8	47.95
168	2.184	0.90	1.80	5.4	9.5	56.84
288	2.37	0.96	1.93	5.8	9.4	61.7

In both mono-layered and bi-layered SDVG the release profile of Fucoïdan shows two separate phases an initial rapid release phase then followed by gradual release phase. The initial rapid burst phase arises due to desorption of surface bound Fucoïdan into the release medium i.e. PBS and also release of Fucoïdan from the hydrophilic PEO component. A considerable fraction of Fucoïdan released in the initial phase is due to degradation of PEO component of the polymer blend. As PEO is hydrophilic it dissolves first in the PBS in course with incubation time. The latter gradual release is ascribed to two different mechanisms, one being diffusion of Fucoïdan from the bulk of fiber into the release medium and other is gradual release of Fucoïdan from slowly degrading PCL component of the polymer blend. This shows the tendency of the PEO: PCL system to act as very good reservoir for Fucoïdan, exhibiting extended, controlled and uniform Fucoïdan release.

Table 4.7: Percentage Fucoïdan release from bi-layered SDVG.

S.No.	% Release of Fucoïdan			Time (hour)	Days
	Sample 1	Sample 2	Sample 3		
1	18	16	18	2	-
2	22	23	21	4	-
3	30	30	33	24	1
4	38	35	36	48	2
5	43	41	44	72	3
6	47	46	48	96	4
7	56	51	52	168	7
8	61	56	59	288	12

The proposed release mechanism was very well supported with the results of DSC analysis, the PEO component of PEO/PCL blend being hydrophilic degrades first and the corresponding T_g for PEO vanishes slowly as the samples are incubated for longer duration in PBS. As this proceeds the bulk sample T_g value tends to move

the corresponding T_g for PEO vanishes slowly as the samples are incubated for longer duration in PBS. As this proceeds the bulk sample T_g value tends to move towards the T_g of PCL with course of incubation time in PBS indicating that it is the PCL component alone that is left in the sample.

Table 4.8: Percentage Fucoïdan release from mono-layered SDVG.

S.No.	% Release of Fucoïdan			Time (hour)	Days
	Sample 1	Sample 2	Sample 3		
1	32.1	31.4	28.8	2	-
2	48.4	44.7	47.3	4	-
3	61.2	56.6	58.5	24	1
4	69.1	65.4	71.9	48	2
5	76.3	74.5	78.7	72	3
6	82.7	80.8	81.3	96	4

Fucoïdan release profile from mono-layered and bi-layered SDVG shows their own characteristic release profile. The significant aspect which could be clearly observed as a matter of contrast between the two is the delayed release of Fucoïdan in bi-layered SDVG when compared to that of mono-layered SDVG. On taking into consideration the homogeneity in the chemical composition of the two structures it can be easily concluded that it is only the structural discrepancy between the two that bring in the difference in release profile. In mono-layered SDVG the Fucoïdan loaded layer is directly exposed in contact with the release medium i.e. PBS hence gives a spiked Fucoïdan release initially. In case of bi-layered SDVG the intermediate Fucoïdan loaded layer comes in contact with PBS at delayed time duration in addition to which the released Fucoïdan has to diffuse through the nanofiberous first layer or second layer gradually. As intimal hyperplasia arises in the latter phase (i.e. roughly around 14 days after) implantation it is required that Fucoïdan delivery system also delivers major extent of Fucoïdan in the later phase of implantation. Hence it is the bi-layered SDVG that would be convenient system to deliver Fucoïdan in phase with the occurrence of intimal hyperplasia after graft implantation in the host.

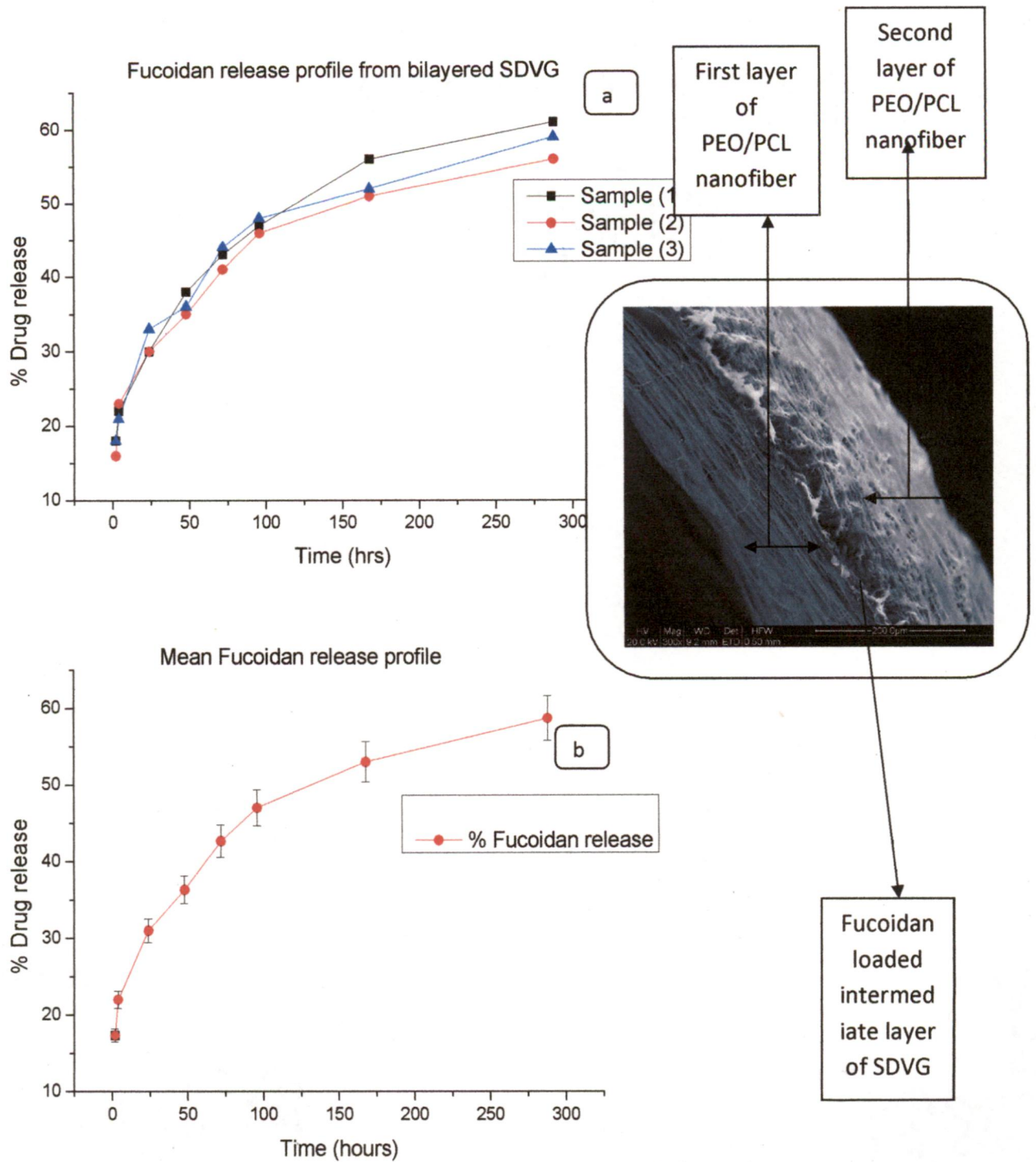


Fig 4.13: Plot of (a) Drug release from bi-layered SDVG in course with incubation tie in PBS and (b) Mean % Fucoidan release with error bar.

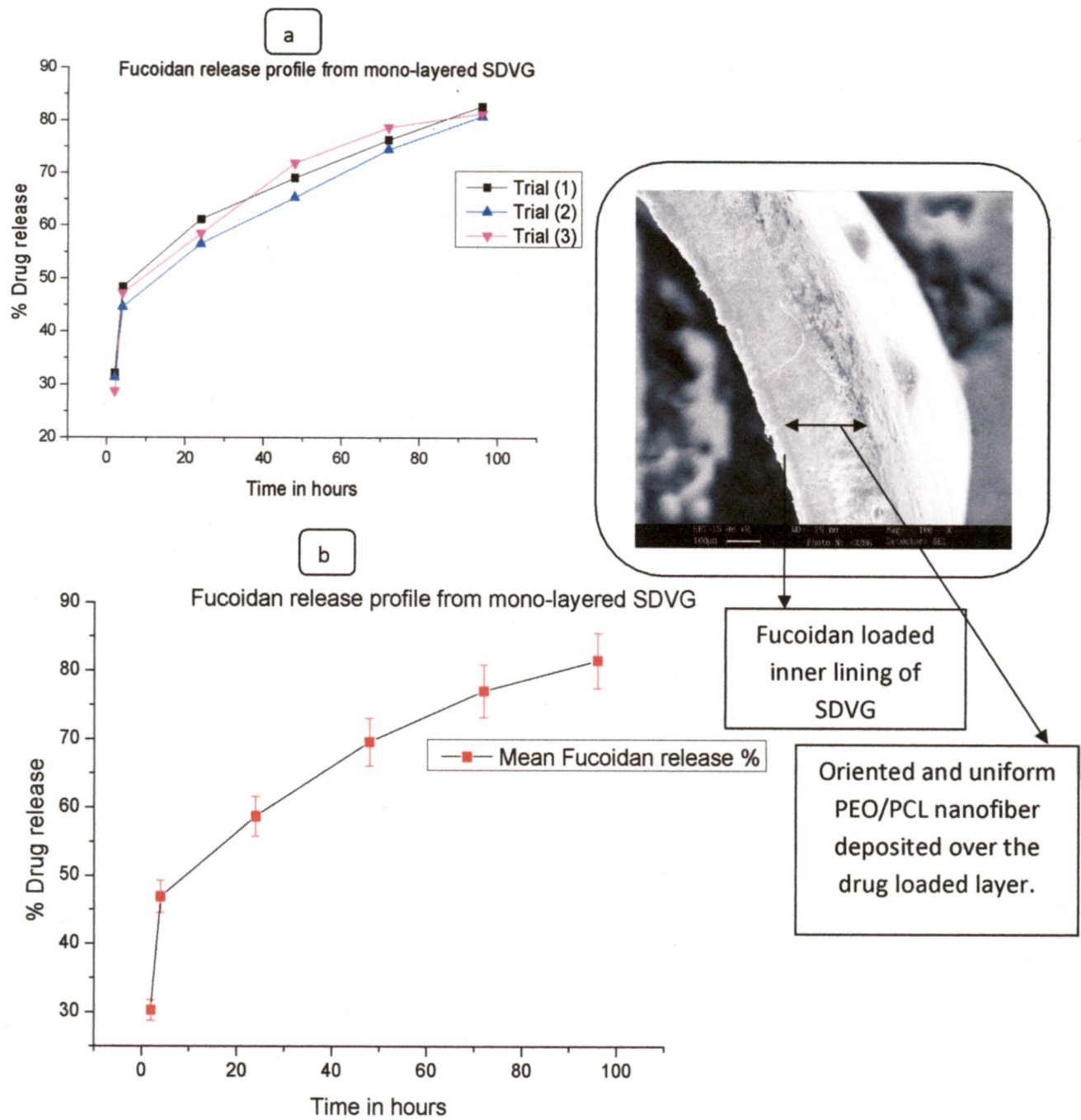


Fig 4.13: Plot of (a) Drug release from mono-layered SDVG in course with incubation tie in PBS and (b) Mean % Fucoidan release with error bar.

The difference in release profile of the mono-layered and bi-layered SDVG also indicates that the release profile of Fucoïdan could also be tailored to desired prolonged time duration by increasing the depth of the Fucoïdan loaded layer away from the inner conduit of the SDVG. The deeper the drug loaded layer more gradual and delayed will be the drug release. Thus the graft could be fabricated as the requirement is, added to this there is also a chance that the mechanical properties deviate to significant extent when the drug loaded layer is varied in depth through the cross-section of the SDVG, hence this has to be ensured to confirm the flexibility of nanofiberous PEO/PCL system for Fucoïdan delivery.

(4.8) Conclusion:

Fucoidan is extracted from brown seaweed *Sargassum weitti* and is then blended with PEO/PCL polymer to form a homogeneous electrospinnable solution. The FTIR analysis establishes that Fucoïdan supplemented to the PEO/PCL polymer blend does not undergo a chemical modification and is held in PEO/PCL phase just by physical dispersion. The bi-layered Fucoïdan loaded vascular PEO/PCL SDVG (5mm diameter) is attained by electrospinning alternatively PEO/PCL blend and Fucoïdan loaded PEO/PCL blend with optimized operating parameters. The mono-layered graft was inculcated with a Fucoïdan loaded luminal surface whereas the bilayerd graft was fabricated with a Fucoïdan loaded intermediated layer. The difference in release profile of the mono-layered and bi-layered SDVG also indicates that the release profile of Fucoïdan could also be tailored to desired prolonged time duration by increasing the depth of the Fucoïdan loaded layer away from the conduit axis.

The study establishes the PEO/PCL bilayered vascular graft as a reservoir of Fucoïdan and thereby gave an improved drug delivery in the later phase of graft implantation. The drug release profile showed two phase of drug release one being an initial burst phase accounting for release of 30% of the loaded Fucoïdan. The initial burst phase is ascribed to the dissolution of loosely bound Fucoïdan and degradation of hydrophilic PEO component in the intermediate layer. The latter sustained Fucoïdan release phase is governed by gradual diffusion of the Fucoïdan and slow degradation of PCL phase. The dimensional uniformity of the vascular graft is confirmed by examining the cross section at different lengths along the graft. The study of interface under SEM showed a good overlap of the intermediate layer with the first and the second layer of PEO/PCL nanofiber. On the whole, the PEO/PCL graft fabricated can be a potential solution for long term patency of SDVG with a controlled and extended drug delivery. A comprehensive study of mechanical compliance and SMC's compatibility with the Fucoïdan loaded PEO/PCL blend can further bolster the application of the scaffold for fabricating SDVG.

References

1. Lloyd-Jones D, Adams RJ, Brown TM, et al, Executive summary: Heart Disease and Stroke Statistics-2010 Update, A report from the American Heart Association Statistics Committee and Stroke Statistics Subcommittee, *Circulation* 2010; 121:948-954.
2. www.texheart surgeons.com/CABG.htm
3. Susan J. Sullivan, Kelvin G. M. Brockbank. Small-Diameter Vascular Grafts. In *Principles of Tissue Engineering*; Robert P. Lanza, Robert Langer, Joseph Vacanti, Eds.; Academic Press: 2000; p 448-449.
4. Peter Zilla, Howard P. Greisler. *Tissue engineering of vascular prosthetic grafts*. R.G.Landes Company, 1999.
5. Weinberg, C.B., and Bell, E. A blood vessel model constructed from collagen and cultured vascular cells, *Science* 1986; 231: 397-400.
- 6 Seal,B.L., Otero,T.C., and Panitch,A. (2001). Polymeric biomaterials for tissue and organ regeneration. *Materials Science & Engineering R-Reports* 34, 147-230.
- 7 Sayers,R.D., Raptis,S., Berce,M., and Miller,J.H. (1998). Long-term results of femorotibial bypass with vein or polytetrafluoroethylene. *British Journal of Surgery* 85, 934-938.
- 8 Ratcliffe,A. (2000). Tissue engineering of vascular grafts. *Matrix Biology* 19, 353-357.
- 9 Thomas,A.C., Campbell,G.R., and Campbell,J.H. (2003). Advances in vascular tissue engineering. *Cardiovascular Pathology* 12, 271-276.
- 10 Kakisis,J.D., Liapis,C.D., Breuer,C., and Sumpio,B.E. (2005). Artificial blood vessel: The Holy Grail of peripheral vascular surgery. *Journal of Vascular Surgery* 41, 349-354.

- 11 Escolar, E., Mintz, G. S., Hong, M.-K., Lee, C. W., Kim, J.-J., Fearnot, N. E., Park, S.-W., et al. (2004). Relation of intimal hyperplasia thickness to stent size in paclitaxel-coated stents. *The American journal of cardiology*, *94*(2), 196-8. doi:10.1016/j.amjcard.2004.03.062
- 12 Feldman, L. J., Aguirre, L., Ziolo, M., Bridou, J.-pierre, Nevo, N., Michel, J.-baptiste, & Steg, P. G. (2000). Interleukin-10 Inhibits Intimal Hyperplasia After Hypercholesterolemic Rabbits, 908-916. doi:10.1161/01.CIR.101.8.908
- 13 Liu, B., Han, M., & Wen, J.-kun. (2008). Acetylbritannilactone Inhibits Neointimal Hyperplasia after Balloon Injury of Rat Artery by Suppressing Nuclear Factor- κ B Activation, *324*(1), 292-298. doi:10.1124/jpet.107.127407.activation
- 14 Lovett, M., Kluge, J., & Vunjak-novakovic, G. (2010). Tubular silk scaffolds for small diameter vascular grafts, (December), 217-224. doi:10.4161/org6.4.13407
- 15 Nyamekye, I., Buonaccorsi, G., McEwan, J., MacRobert, a, Bown, S., & Bishop, C. (1996). Inhibition of intimal hyperplasia in balloon injured arteries with adjunctive phthalocyanine sensitised photodynamic therapy. *European journal of vascular and endovascular surgery*: the official journal of the European Society for Vascular Surgery, *11*(1), 19-28. Retrieved from <http://www.ncbi.nlm.nih.gov/pubmed/8564482>
- 16 Rekhater, M. D. (1999). Collagen synthesis in atherosclerosis: too much and not enough. *Cardiovascular research*, *41*(2), 376-84. Retrieved from <http://www.ncbi.nlm.nih.gov/pubmed/10341837>
- 17 Roy-Chaudhury, P. (2005). Endothelial progenitor cells, neointimal hyperplasia, and hemodialysis vascular access dysfunction: novel therapies for a recalcitrant clinical problem. *Circulation*, *112*(1), 3-5. doi:10.1161/CIRCULATIONAHA.105.548651
- 18 Skalský, I., Filová, E., Szárszoi, O., Pařízek, M., & Lytvynets, A. (2011). RAPID COMMUNICATION A Periadventitial Sirolimus-Releasing Mesh Decreased Intimal Hyperplasia in a Rabbit Model, *8408*, 585-588.
- 19 Soletti, L., Hong, Y., Guan, J., Stankus, J. J., & El-kurdi, M. S. (2010). Acta Biomaterialia A bilayered elastomeric scaffold for tissue engineering of small diameter vascular grafts. *Acta Biomaterialia*, *6*(1), 110-122. Acta Materialia Inc. doi:10.1016/j.actbio.2009.06.026
- 20 Teebken, O. E., & Haverich, A. (2002). Tissue Engineering of Small-Diameter Vascular Grafts.

- 21 Wu, J., & Zhang, C. (2009). Neointimal hyperplasia, vein graft remodeling, and long-term patency. *American journal of physiology. Heart and circulatory physiology*, 297(4), H1194-5. doi:10.1152/ajpheart.00703.2009
- 22 Ã, O. E. T., & Haverich, A. (2002). Tissue Engineering of Small Diameter Vascular Grafts. *European Journal of Vascular and Endovascular Surgery*, 485.
22. Weinberg CB, Bell E. A blood vessel model constructed from collagen and cultured vascular cells. *Science*. 1986, 231: 397-400.
23. L'Heureux N, Germain L, Labbé R, Auger FA. In vitro construction of a human blood vessel from cultured vascular cells: a morphologic study. *J Vasc Surg*. 1993 Mar;17(3):499-509.
24. L'Heureux N, Pâquet S, Labbé R, Germain L, Auger FA. A completely biological tissue-engineered human blood vessel. *FASEB J*. 1998 Jan;12(1):47-56.
- 25: Konig G, McAllister TN, Dusserre N, Garrido SA, Iyican C, Marini A, Fiorillo A, Avila H, Wystrychowski W, Zagalski K, Maruszewski M, Jones AL, Cierpka L, de la Fuente LM, L'Heureux N. Mechanical properties of completely autologous human tissue engineered blood vessels compared to human saphenous vein and mammary artery. *Biomaterials*. 2009 Mar;30(8):1542-50.
26. McAllister TN, Maruszewski M, Garrido SA, Wystrychowski W, Dusserre N, Marini A, Zagalski K, Fiorillo A, Avila H, Manglano X, Antonelli J, Kocher A, Zembala M, Cierpka L, de la Fuente LM, L'heureux N. Effectiveness of haemodialysis access with an autologous tissue-engineered vascular graft: a multicentre cohort study. *Lancet*. 2009 Apr 25;373(9673):1440-6.
27. Keire PA, L'Heureux N, Vernon RB, Merrilees MJ, Starcher B, Okon E, Dusserre N, McAllister TN, Wight TN. Expression of versican isoform V3 in the absence of ascorbate improves elastogenesis in engineered vascular constructs. *Tissue Eng Part A*. 2010 Feb;16(2):501-12.
28. Ziegler T and Nerem RM. Tissue engineering a blood vessel: Regulation of vascular biology by mechanical stresses. *J Cell Biochem*. 56, 204-209.
- 29: Seliktar D, Black RA, Vito RP, Nerem RM. Dynamic mechanical conditioning of collagen-gel blood vessel constructs induces remodeling in vitro. *Ann Biomed Eng*, 2000, 28, 351-362.
30. Ahsan T, Nerem RM. Fluid shear stress promotes an endothelial-like phenotype during the early differentiation of embryonic stem cells. *Tissue Eng Part A*. 2010 Nov;16(11):3547-53.

31. Huynh T, Abraham G, Murray J, Brockbank K, Hagen PO, Sullivan S. Remodeling of an acellular collagen graft into a physiologically responsive neovessel. *Nat Biotechnol.* 1999 Nov;17(11):1083-6.
32. Lu Q, Ganesan K, Simionescu DT, Vyavahare NR. Novel porous aortic elastin and collagen scaffolds for tissue engineering. *Biomaterials.* 2004 97 Oct;25(22):5227-37.
33. Dahl SL, Koh J, Prabhakar V, Niklason LE. Decellularized native and engineered arterial scaffolds for transplantation. *Cell Transplant.* 2003;12(6):659-666.
34. Amiel GE, Komura M, Shapira O, Yoo JJ, Yazdani S, Berry J, Kaushal S, Bischoff J, Atala A, Soker S. Engineering of blood vessels from acellular collagen matrices coated with human endothelial cells. *Tissue Eng.* 2006 Aug;12(8):2355-65.
35. Blakemore, A.H. and Voorhees, A.B. Jr. (1954). The use of tubes constructed from vinylon N cloth in bridging arterial defects; experimental and clinical. *Annals of Surgery* 140, 324-334.
36. Hastings, G.W. (1992). Preface. In: *Cardiovascular biomaterials*, ed. G.W. Hastings. New York: Springer-Verlag.
37. Vroman, L.M. and Adams, A.L. (1969). Identification of rapid changes at plasma-solid interfaces. *Journal of Biomedical Materials Research* 3, 43-67.
38. Matsuda, T. (2004). Recent progress of vascular graft engineering in Japan. *Artificial Organs* 28, 64-71.
39. Sayers, R.D., Raptis, S., Berce, M., and Miller, J.H. (1998). Long-term results of femorotibial bypass with vein or polytetrafluoroethylene. *British Journal of Surgery* 85, 934-938.
40. Seal, B.L., Otero, T.C., and Panitch, A. (2001). Polymeric biomaterials for tissue and organ regeneration. *Materials Science & Engineering R-Reports* 34, 147-230.
41. William, J.M. Methods of dispersing fluids. [705,691], 1-4. 1902. New York/USA. Ref Type: Patent
42. Xu, C.Y., Inai, R., Kotaki, M., and Ramakrishna, S. (2004b). Electrospun nanofiber fabrication as synthetic extracellular matrix and its potential for vascular tissue engineering. *Tissue Engineering* 10, 1160-1168.
43. Yarin, A.L., Koombhongse, S., and Reneker, D.H. (2001). Bending instability in electrospinning of nanofibers. *Journal of Applied Physics* 89, 3018-3026.

- 44 Ma,Z.W., Kotaki,M., Inai,R., and Ramakrishna,S. (2005b). Potential of nanofiber matrix as tissue-engineering scaffolds. *Tissue Engineering* 11, 101-109.
- 45 Lutolf,M.P. and Hubbell,J.A. (2005). Synthetic biomaterials as instructive extracellular microenvironments for morphogenesis in tissue engineering. *Nature Biotechnology* 23, 47-55.
- 46 Alberts,B., Johnson,A., Lewis,J., Raff,M., Roberts,K., and Walter,P. (2002). Cells in Their Social Context. In: *Molecular Biology of Cell*. New York: Garland Science, 1065-1125.
- 47 Nishida,T., Yasumoto,K., Otori,T., and Desaki,J. (1988). The Network Structure of Corneal Fibroblasts in the Rat As Revealed by Scanning Electron-Microscopy. *Investigative Ophthalmology & Visual Science* 29, 1887-1890.
- 48 Cao,Y.L., Vacanti,J.P., Paige,K.T., Upton,J., and Vacanti,C.A. (1997). Transplantation of chondrocytes utilizing a polymer-cell construct to produce tissue-engineered cartilage in the shape of a human ear. *Plastic and Reconstructive Surgery* 100, 297-302.
- 49 Matthews,J.A., Boland,E.D., Wnek,G.E., Simpson,D.G., and Bowlin,G.L. (2003). Electrospinning of collagen type II: A feasibility study. *Journal of Bioactive and Compatible Polymers* 18, 125-134.
- 50 Kim,H.W., Song,J.H., and Kim,H.E. (2005a). Nanoriber generation of gelatinhydroxyapatite biomimetics for guided tissue regeneration. *Advanced Functional Materials* 15, 1988-1994.
- 51 Jin,H.J., Chen,J.S., Karageorgiou,V., Altman,G.H., and Kaplan,D.L. (2004). Human bone marrow stromal cell responses on electrospun silk fibroin mats. *Biomaterials* 25, 1039-1047.
- 52 Unger,R.E., Peters,K., Huang,Q., Funk,A., Paul,D., and Kirkpatrick,C.J. (2005). Vascularization and gene regulation of human endothelial cells growing on porous polyethersulfone (PES) hollow fiber membranes. *Biomaterials* 26, 3461-3469.
- 53 Fang,X. and Reneker,D.H. (1997). DNA fibers by electrospinning. *Journal of Macromolecular Science-Physics* B36, 169-173.
- 54 Luu,Y.K., Kim,K., Hsiao,B.S., Chu,B., and Hadjiargyrou,M. (2003). Development of a nanostructured DNA delivery scaffold via electrospinning of PLGA and PLA-PEG block copolymers. *Journal of Controlled Release* 89, 341-353.

- 55 Giliberti,D.C., White,K.K., and Dee,K.C. (2002). Control of Cell-Biomaterials Interactions. In: Polymeric biomaterials, ed. S.DumitriuNew York: Marcel Dekker Inc. 361-375.
- 56 Rosenberg,M.D. (1963). Cell guidance by alterations in monomolecular films. *Science* 139, 411-412.
- 57Laurencin,C.T., Ambrosio,A.M.A., Borden,M.D., and Cooper,J.A. (1999). Tissue engineering: Orthopedic applications. *Annual Review of Biomedical Engineering* 1, 19-46.
- 58 Fan,Y.W., Cui,F.Z., Hou,S.P., Xu,Q.Y., Chen,L.N., and Lee,I.S. (2002). Culture of neural cells on silicon wafers with nano-scale surface topograph. *Journal of Neuroscience Methods* 120, 17-23.
- 59 Elias,K.L., Price,R.L., and Webster,T.J. (2002). Enhanced functions of osteoblasts on nanometer diameter carbon fibers. *Biomaterials* 23, 3279-3287.
- 60 Hashi, C.K., Zhu, Y., Yang, G.Y., Young, W.L., Hsiao, B.S., Wang, K., Chu, B., and Li, S. (2007) Antithrombogenic property of bone marrow mesenchymal stem cells in nanofibrous vascular grafts. *Proceedings of the National Academy of Sciences* 104, 11915-11920.
- 61 www.infrared.als.lbl.gov/BLManual. (1820). -1 . 2. *Main*.
- 62 Coates, J., Ed. R. A. M., & Coates, J. (2000). Interpretation of Infrared Spectra , A Practical Approach Interpretation of Infrared Spectra , A Practical Approach. *Interpretation A Journal Of Bible And Theology*, 10815-10837.
- 63 Kaputskii, F. N., Torgashov, V. I., Yurkshtovich, T. L., Golub, N. V., Ostrovskaya, I. L., & Alinovskaya, V. A. (2007). Sulfation of Polysaccharides with Sodium Pyrosulfate in Dimethyl Sulfoxide t h. *Russian Journal of Applied Chemistry*, 80(10), 1745-1749.
- 64 Pereira, L., Amado, A. M., Critchley, A. T., Velde, F. V. D., & Ribeiro-claro, P. J. A. (2009). Food Hydrocolloids Identification of selected seaweed polysaccharides (phycocolloids) by vibrational spectroscopy (FTIR-ATR and FT-Raman. *Food hydrocolloids*, 1-7.